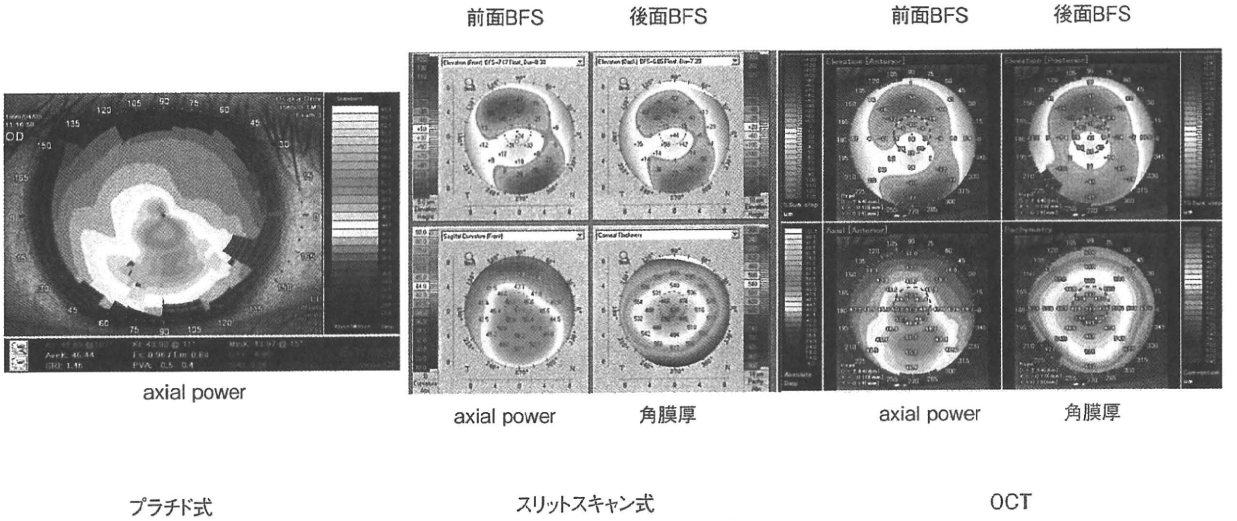

図 29　3種類の装置による円錐角膜の角膜形状解析.
左からプラチド式，スリットスキャン式，およびOCTで測定した結果であり，すべて同一スケールで表示している．いずれも類似したパターンを呈している．
（文献62から許可を得て転載，改変）

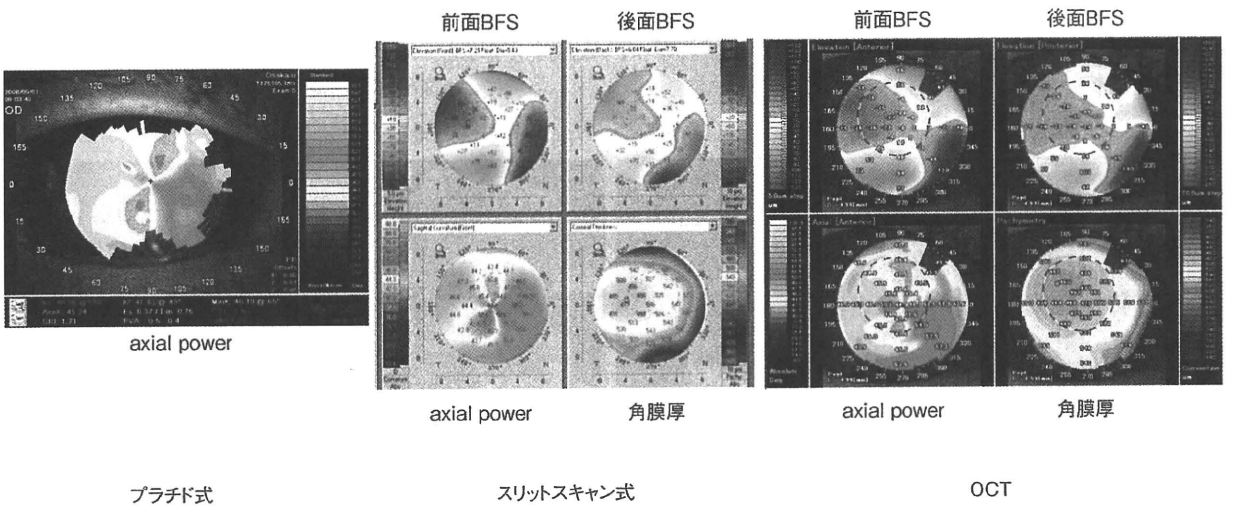

図 30　3種類の装置による全層角膜移植後の角膜形状解析.
左からプラチド式，スリットスキャン式，およびOCTで測定した結果であり，すべて同一スケールで表示している．スリットスキャン式，およびOCTは類似しており，プラチド式は測定範囲が狭い．
（文献62から許可を得て転載，改変）

そこで，swept-sourceの前眼部OCTであるSS-1000(株式会社トーメーコーポレーション，名古屋)をOCT角膜トポグラファーとして使用することを試みた．

使用した装置は，波長が1,310 nm，速度は30,000 A-Scan/秒で，解像度が10 μmである．角膜形状解析の際には，測定パラメーターとして，スキャンモードをRadial，1断面での測定点を前後面とも512点に設定して，16断面を用いて角膜前後面の立体再構築を行った．すなわち前後面とも測定点は最大8,192点とした．その測定径を10 mmとして，測定時間は0.34秒になる．

図29に，中等度円錐角膜眼での，プラチド式角膜トポグラファーのTMS-4 Advance(株式会社トーメーコーポレーション，名古屋)，スリットスキャン式のPentacam HR，およびSS-1000による角膜形状の測定結果を示す．角膜前面のaxial powerマップでは3者が，前後面のエレベーションマップと角膜厚分布では2者が似たパターンを示した．図30は，全層角膜移植後の症例で，同様に角膜形状解析を施行した結果である．角膜前面のaxial powerマップでは3者がやはり大変似たパターンが示した．プラチド式の場合には，宿主母角膜接合部より外側が解析不可能であったが，スリットスキャン式およびOCT式では，その周辺を含めて解析が可能であっ

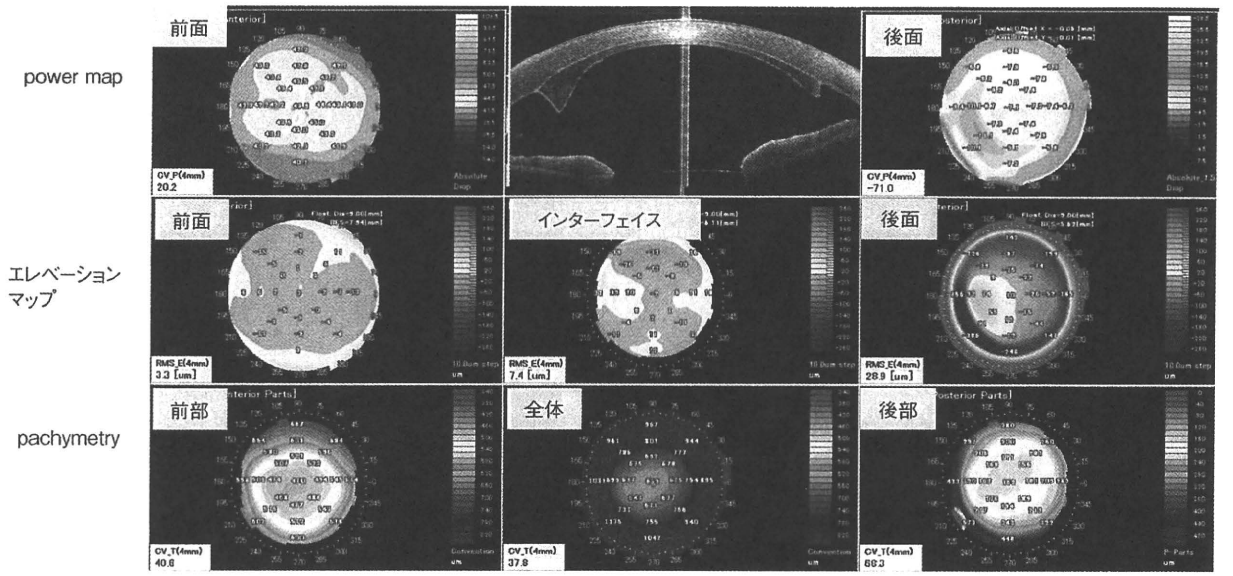

図 31 角膜内皮移植術後の OCT による角膜形状解析.
上段は左から，角膜前面の axial power map，OCT 断面像，角膜後面の axial power map．中段は左から，角膜前面の BFS(best fit sphere)のエレベーションマップ，インターフェイスの BFS のエレベーションマップ，角膜後面の BFS のエレベーションマップ．下段は，左から，母角膜の角膜厚分布，全体の角膜厚分布，およびドナーの角膜厚分布を示す．グラフトの厚みが耳側と鼻側で非対称になり，power map や角膜後面のエレベーションマップが非対称のパターンになっていることが分かる．
(文献 62 から許可を得て転載，改変)

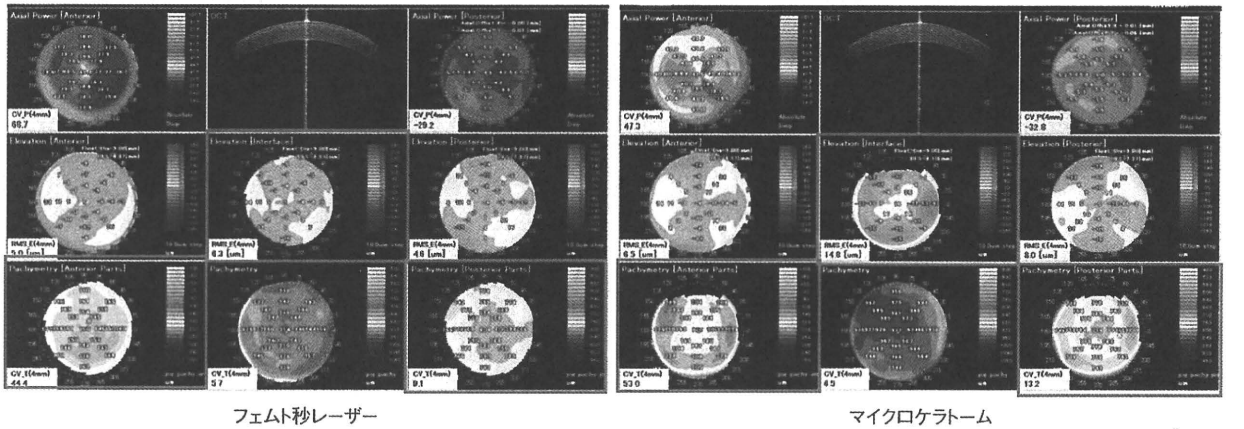

図 32 OCT による角膜形状解析を用いた LASIK におけるフラップ形状の比較.
左はフェムト秒レーザー，右はマイクロケラトームを用いた症例．赤枠で示した中段中央のインターフェイスの BFS のエレベーションマップおよび下段左のフラップの角膜厚分布にて，フェムト秒レーザーが planar flap，マイクロケラトームが meniscus flap のパターンを示しており，下段ベッドの角膜厚分布のパターンが逆転している．
(文献 62 から許可を得て転載，改変)

た．さらに前後面のエレベーションマップと角膜厚分布では 2 者が似たパターンを示した．このように，OCT 角膜トポグラファーは既存の装置と比較して遜色ない程度の測定が可能であった．

プラチド式角膜形状解析装置は，角膜にプラチドリング照明を投影した際に生じる Purkinje 第一像であるマイヤー像を使用しているため，撮影が高速で，軽微な角膜形状の歪みも鋭敏にとらえられるが，マイヤー像が高度に歪んだり，角膜に混濁があると正確な測定ができない，あるいは測定が角膜前面に限られるという問題点がある．一方，スリットスキャン式の装置においては，Scheimpflug 像などのスリット光を走査することによって，角膜前後面の高さの情報を取得し，角膜の三次元立体再構築をしている．その結果，角膜前面だけでなく，

角膜後面や角膜厚の解析も可能である．ただし，プラチド式より測定時間が長い，角膜の混濁があるとやはりその部位の測定が困難になるという問題点がある．

その点，波長1,310 nmの前眼部OCTを用いれば，赤外光で測定中羞明がなく，断面画像の走査も機械的でないため，測定時間を短縮することが可能である．加えて，混濁した角膜への光の深達性が可視光に比較して有利であり，角膜浮腫や瘢痕のある症例での角膜形状解析を行ううえで既存の装置と比較しても有利と考えられる．今まででは角膜形状解析が困難であった高度の角膜不正乱視の症例にも今後角膜形状解析が施行できる可能性があり，その有効性に関して今後検討がなされるべきである．

ところで角膜移植の領域において，近年の角膜内皮移植術や深層層状角膜移植術といった層状角膜移植，いわゆるパーツ移植の発展には目を見張るものがある．全層移植術と比較してこれらの層状移植術の利点，欠点は母角膜と移植片の境界に由来している．しかしながら従来の角膜トポグラファーでは，そのインターフェイスの前後を個別に解析することは不可能であったが，前眼部OCTであればインターフェイスを容易に視認することができる．そこでOCT角膜トポグラファーによって角膜層状手術の評価を試みるべく，その解析方法の開発を行った．

図31は，DSAEK後の症例である．上段中央のOCT断面像に示す如く，ホストとグラフトの境界を認識することによって，今まで不可能であったインターフェイスのエレベーションマップ，ホストとグラフトを別個に角膜厚マップとして表示することが可能となり，さらにそれぞれのマップに対して指数を開発して定量的解析を施行することができる．この症例においてはグラフトが偏心して切除され厚みが非対称になっていることが分かる．

このようにOCT角膜トポグラファーを用いれば，層状角膜移植術をより詳細に定量的に解析することが可能であり，その術式の成績の向上や改良に有用な可能性がある．また，pre-cutドナーの切開の状態などを術前に評価することが可能であり，今後の検討が待たれる．

角膜にインターフェイスのある状態としてLASIKがある．今回開発した方法を用いれば，そのフラップの形状を評価することも可能と考えられる．現在，LASIKにおいてフラップを作製する方法としては，マイクロケラトームを用いる方法とフェムト秒レーザーを用いる方法があり，生じるフラップの形状は異なることが知られている．フェムト秒レーザーでは厚みが均一なplanar flapになり，その辺縁は鈍角となるが，マイクロケラトームでは中央が薄いmeniscus flapで辺縁が鋭角であるとされている．図32は，フェムト秒レーザーとして，IntraLase FS®レーザー(エイエムオー・ジャパン株式会社，東京)ないしマイクロケラトームM2(株式会社モリア・ジャパン，東京)を使用し，VISXエキシマレーザーシステムSTAR S4IR®(エイエムオー・ジャパン株式会社，東京)でLASIKを施行した代表的症例である．フラップの角膜厚マップによってフェムト秒レーザーでは厚みが比較的均一であるが，マイクロケラトームでは中央が薄くなっていることが示される．

このようにインターフェイスを立体として解析することによって，フェムト秒レーザーとマイクロケラトームの面精度を指数として定量的に解析することも可能であり，今後症例を増やし検討する必要があるがこの2例に限れば，フェムト秒レーザーはよりplanar flapであることが示唆された．

以上，swept-source OCTをOCT角膜トポグラファーとして使用したところ，従来の角膜トポグラファーで困難な混濁が強い部位の解析や，インターフェイスの形状解析が可能で，高度の角膜形状異常の解析や層状角膜移植術やLASIKなど角膜層状手術の評価に有用と考えられた．

Ⅵ　おわりに

眼科臨床は，検査によって，診断・重症度の判定，治療法の適応，治療法を選択し，次いで治療効果の判定，結果をフィードバックすることで進歩しているのは疑いもない事実であって，今後もできるだけ侵襲の少ない，そして治療法選択を支えることが可能な検査をさらに開発し，検査と治療の繰り返しを続けることが，独創的な治療を，リスクを低減しつつ標準化するために最良の方法ではないかと考えられる．

細隙灯顕微鏡検査および視力検査は，前眼部疾患の診断に最も有用なものであるが，治療の進歩に伴い，その弱点を補う相補的な検査が必要となっている．今回施行した高次収差の定量的解析により，角膜形状異常診断，不正乱視の視機能への影響評価，眼内レンズ，コンタクトレンズ，屈折矯正手術のテーラーメイド治療を容易にできる可能性がある．さらに，高次収差を連続測定することにより，涙液やコンタクトレンズによる視覚の質の動的変化が評価できる．Full-field OCTで角膜の細胞レベルの経時的観察が可能であり，OCT角膜トポグラファーは，角膜層状手術の評価に有用な可能性があり，今後の発展が望まれる．

本講演の機会をお与えいただいた日本眼科学会評議員の先生方，第114回日本眼科学会総会総会長の寺崎浩子名古屋大学教授，座長の労をおとりいただいた大鹿哲郎筑波大学教授に厚く御礼申し上げます．

長年に亘り多大なご支援をいただいております大阪大学眼科学教室同窓会の諸先生方，大阪府眼科医会の先生方に心より感謝を申し上げます．

稿を終えるにあたり，私の恩師であり，常に貴重なご助言

と暖かい励ましの言葉を与えてくださいました眞鍋禮三大阪大学名誉教授，Stephen D Klyce 教授(Mount Sinai 医科大学)，ならびに故田野保雄大阪大学前教授に深甚の謝意を表します．

今回の研究は，科学研究費補助金(基盤C)より補助金を受け，日本眼科学会評議員会賞より支援を受けました．

本総説は第114回日本眼科学会総会評議員会指名講演の内容に基づいて執筆いたしましたが，講演内容の一部は現在投稿中であり，本稿から割愛させていただきましたことをお詫び申し上げます．

利益相反：前田直之(カテゴリーF：トプコン，トーメーコーポレーション)

文　献

1) **Duke-Elder S, Smith RJH**：The examination of the eye. In：Duke-Elder S(Ed)：System of Ophthalmology, vol Ⅶ The Foundations of Ophthalmology. Henry Kimpton, London, 233—281, 1962.
2) **Wilson SE, Klyce SD**：Screening for corneal topographic abnormalities before refractive surgery. Ophthalmology 101：147—152, 1994.
3) **Mishima S**：Clinical investigations on the corneal endothelium-XXXVIII Edward Jackson Memorial Lecture. Am J Ophthalmol 93：1—29, 1982.
4) **Klyce SD**：Computer-assisted corneal topography. High-resolution graphic presentation and analysis of keratoscopy. Invest Ophthalmol Vis Sci 25：1426—1435, 1984.
5) **Liang J, Grimm B, Goelz S, Bille JF**：Objective measurement of wave aberrations of the human eye with the use of a Hartmann-Shack wave-front sensor. J Opt Soc Am A 11：1949—1957, 1994.
6) **Lemp MA, Dilly PN, Boyde A**：Tandem-scanning (confocal) microscopy of the full-thickness cornea. Cornea 4：205—209, 1986.
7) **Izatt JA, Hee MR, Swanson EA, Lin CP, Huang D, Schuman JS,** et al：Micrometer-scale resolution imaging of the anterior eye *in vivo* with optical coherence tomography. Arch Ophthalmol 112：1584—1589, 1994.
8) **Mrochen M, Kaemmerer M, Seiler T**：Wavefront-guided laser *in situ* keratomileusis：early results in three eyes. J Refract Surg 16：116—121, 2000.
9) **Holladay JT, Piers PA, Koranyi G, van der Mooren M, Norrby NE**：A new intraocular lens design to reduce spherical aberration of pseudophakic eyes. J Refract Surg 18：683—691, 2002.
10) **Maeda N**：Wavefront technology in ophthalmology. Curr Opini Ophthalmol 12：294—299, 2001.
11) **Kuroda T, Fujikado T, Maeda N, Oshika T, Hirohara Y, Mihashi T**：Wavefront analysis of higher-order aberrations in patients with cataract. J Cataract Refract Surg 28：438—444, 2002.
12) **Kuroda T, Fujikado T, Ninomiya S, Maeda N, Hirohara Y, Mihashi T**：Effect of aging on ocular light scatter and higher order aberrations. J Refract Surg 18：S 598—602, 2002.
13) **Ninomiya S, Maeda N, Kuroda T, Saito T, Fujikado T, Tano Y,** et al：Clinicopathologic reports, case reports, and small case series：evaluation of lenticular irregular astigmatism using wavefront analysis in patients with lenticonus. Arch Ophthalmol 120：1388—1393, 2002.
14) **Maeda N, Fujikado T, Kuroda T, Mihashi T, Hirohara Y, Nishida N,** et al：Wavefront aberrations measured with Hartmann-Shack sensor in patients with keratoconus. Ophthalmology 109：1996—2003, 2002.
15) **Koh S, Maeda N, Kuroda T, Hori Y, Watanabe H, Fujikado T,** et al：Effect of tear film break-up on higher-order aberrations measured with wavefront sensor. Am J Ophthalmol 134：115—117, 2002.
16) **Ninomiya S, Maeda N, Kuroda T, Fujikado T, Tano Y**：Comparison of ocular higher-order aberrations and visual performance between photorefractive keratectomy and laser *in situ* keratomileusis for myopia. Semin Ophthalmol 18：29—34, 2003.
17) **Ninomiya S, Fujikado T, Kuroda T, Maeda N, Tano Y, Hirohara Y,** et al：Wavefront analysis in eyes with accommodative spasm. Am J Ophthalmol 136：1161—1163, 2003.
18) 大鹿哲郎：眼科検査診断法．視覚の質 quality of vision を測る．日眼会誌 108：770—808, 2004.
19) 不二門　尚：眼科検査診断法．新しい視機能評価システムの開発．日眼会誌 108：809—835, 2004.
20) **Fujikado T, Kuroda T, Maeda N, Kim A, Tano Y, Oshika T,** et al：Wavefront analysis of an eye with monocular triplopia and nuclear cataract. Am J Ophthalmol 137：361—363, 2004.
21) **Fujikado T, Kuroda T, Maeda N, Ninomiya S, Goto H, Tano Y,** et al：Light scattering and optical aberrations as objective parameters to predict visual deterioration in eyes with cataracts. J Cataract Refract Surg 30：1198—1208, 2004.
22) **Fujikado T, Kuroda T, Ninomiya S, Maeda N, Tano Y, Oshika T,** et al：Age-related changes in ocular and corneal aberrations. Am J Ophthalmol 138：143—146, 2004.
23) **Kim A, Bessho K, Okawa Y, Maeda N, Tano Y, Hirohara Y,** et al：Wavefront analysis of eyes with cataracts in patients with monocular triplopia. Ophthal Physiol Opt 26：65—70, 2006.
24) **Fujikado T, Shimojyo H, Hosohata J, Hirohara Y, Mihashi T, Maeda N,** et al：Wavefront analysis of eye with monocular diplopia and cortical cataract. Am J Ophthalmol 141：1138—1140, 2006.
25) **Takehara A, Maeda N, Ninomiya S, Fujikado T, Hirohara Y, Mihashi T**：Effects of reference axes used during measurements of ocular and corneal

higher-order aberrations in patients following LASIK. Jpn J Ophthalmol 50：318—322, 2006.
26) **Mihashi T, Hirohara Y, Bessho K, Maeda N, Oshika T, Fujikado T**：Intensity analysis of Hartmann-Shack images in cataractous, keratoconic, and normal eyes to investigate light Scattering. Jpn J Ophthalmol 50：323—333, 2006.
27) **Hirohara Y, Mihashi T, Suzaki A, Kuroda T, Kelly JE, Maeda N**, et al：Evaluating optical quality of a bifocal soft contact lens in near vision using a Shack-Hartmann wavefront sensor. Optical Review 13：396—404, 2006.
28) **Mihashi T, Hirohara Y, Koh S, Ninomiya S, Maeda N, Fujikado T**：Tear film break-up time evaluated by real-time Hartmann-Shack wavefront sensing. Jpn J Ophthalmol 50：85—89, 2006.
29) **Maeda N**：Topcon KR-9000PW. In：Wang W (Ed)：Corneal topography in the wavefront era a guide for clinical application. SLACK Incorporated, Thorofare, 259—267, 2006.
30) **Maeda N**：Clinical application of wavefront aberrometry-A review. Clini Experiment Ophthalmol 37：118—129, 2009.
31) **Campbell CE**：A new method for describing the aberrations of the eye using Zernike polynomials. Optom Vis Sci 80：79—83, 2003.
32) **Kosaki R, Maeda N, Bessho K, Hori Y, Nishida K, Suzaki A**, et al：Magnitude and orientation of Zernike terms in patients with keratoconus. Invest Ophthalmol Vis Sci 48：3062—3068, 2007.
33) **Negishi K, Kumanomido T, Utsumi Y, Tsubota K**：Effect of higher-order aberrations on visual function in keratoconic eyes with a rigid gas permeable contact lens. Am J Ophthalmol 144：924—929, 2007.
34) **Chen M, Yoon G**：Posterior corneal aberrations and their compensation effects on anterior corneal aberrations in keratoconic eyes. Invest Ophthalmol Vis Sci 49：5645—5652, 2008.
35) **Nakagawa T, Maeda N, Kosaki R, Hori Y, Inoue T, Saika M**, et al：Higher-order aberrations due to the posterior corneal surface in patients with keratoconus. Invest Ophthalmol Vis Sci 50：2660—2665, 2009.
36) **Kelly JE, Mihashi T, Howland HC**：Compensation of corneal horizontal/vertical astigmatism, lateral coma, and spherical aberration by internal optics of the eye. J Vis 4：262—271, 2004.
37) **Tang M, Shekhar R, Miranda D, Huang D**：Characteristics of keratoconus and pellucid marginal degeneration in mean curvature maps. Am J Ophthalmol 140：993—1001, 2005.
38) **Kamiya K, Hirohara Y, Mihashi T, Hiraoka T, Kaji Y, Oshika T**：Progression of pellucid marginal degeneration and higher-order wavefront aberration of the cornea. Jpn J Ophthalmol 47：523—525, 2003.
39) **Oie Y, Maeda N, Kosaki R, Suzaki A, Hirohara Y, Mihashi T**, et al：Characteristics of ocular higher-order aberrations in patients with pellucid marginal corneal degeneration. J Cataract Refract Surg 34：1928—1934, 2008.
40) **Kosaki R, Maeda N, Hayashi H, Fujikado T, Okamoto S**：Effect of NIDEK optimized aspheric transition zone ablation profile on higher order aberrations during LASIK for myopia. J Refract Surg 25：331—338, 2009.
41) 前田直之：角膜形状からみた眼内レンズ選択．眼科手術21：309—315, 2008.
42) **McQueen BR, Martinez CE, Klyce SD**：Corneal topography in cataract surgery. Curr Opin Ophthalmol 8：22—28, 1997.
43) **Eppig T, Scholz K, Langenbucher A**：Assessing the optical performance of multifocal (diffractive) intraocular lenses. Ophthalmic Physiol Opt 28：467—474, 2008.
44) **Seitz B, Langenbucher A**：Intraocular lens power calculation in eyes after corneal refractive surgery. J Refract Surg 6：349—361, 2000.
45) **Wang L, Hill WE, Koch DD**：Evaluation of intraocular lens power prediction methods using the American Society of Cataract and Refractive Surgeons Post-Keratorefractive Intraocular Lens Power Calculator. J Cataract Refract Surg 36：1466—1473, 2010.
46) **Koh S, Maeda N, Hirohara Y, Mihashi T, Ninomiya S, Bessho K**, et al：Serial measurements of higher-order aberrations after blinking in normal subjects. Invest Ophthalmol Vis Sci 47：3318—3324, 2006.
47) **Tsubota K, Nakamori K**：Dry eyes and video display terminals. N Engl J Med 328：584, 1993.
48) **Goto T, Zheng X, Klyce SD, Kataoka H, Uno T, Karon M**, et al：A new method for tear film stability analysis using videokeratography. Am J Ophthalmol 135：607—612, 2003.
49) **Koh S, Maeda N, Hori Y, Inoue T, Watanabe H, Hirohara Y**, et al：Effects of suppression of blinking on quality of vision in borderline cases of evaporating dry eye. Cornea 27：275—278, 2008.
50) **Koh S, Maeda N, Hirohara Y, Mihashi T, Bessho K, Hori Y**, et al：Serial measurements of higher-order aberrations after blinking in patients with dry eye. Invest Ophthalmol Vis Sci 49：133—138, 2008.
51) **Montés-Micó R, Alió JL, Charman WN**：Dynamic changes in the tear film in dry eyes. Invest Ophthalmol Vis Sci 46：1615—1619, 2005.
52) **Koh S, Maeda N, Ninomiya S, Watanabe H, Fujikado T, Tano Y**, et al：Paradoxical increase of visual impairment with punctal occlusion in a patient with mild dry eye. J Cataract Refract Surg 32：689—691, 2006.
53) **King-Smith PE, Fink BA, Hill RM, Koelling KW, Tiffany JM**：The thickness of the tear film. Curr

Eye Res 29 : 357—368, 2004.
54) **Koh S, Maeda N, Hamano T, Hirohara Y, Mihashi T, Hori Y,** et al : Effects of internal lubricating agents of disposable soft contact lenses on higher-order aberrations after blinking. Eye & Contact Lens 34 : 100—105, 2008.
55) **Hirohara Y, Mihashi T, Koh S, Ninomiya S, Maeda N, Fujikado T** : Optical quality of the eye degraded by time-varying wavefront aberrations with tear film dynamics. Jpn J Ophthalmol 51 : 258—264, 2007.
56) **Huang D, Swanson EA, Lin CP, Schuman JS, Stinson WG, Chang W,** et al : Optical coherence tomography. Science 254 : 1178—1181, 1991.
57) **Konstantopoulos A, Hossain P, Anderson DF** : Recent advances in ophthalmic anterior segment imaging : a new era for ophthalmic diagnosis? Br J Ophthalmol 91 : 551—557, 2007.
58) **Chen J, Lee L** : Clinical applications and new developments of optical coherence tomography : an evidence-based review. Clin Exp Optom 90 : 317—335, 2007.
59) **Simpson T, Fonn D** : Optical coherence tomography of the anterior segment. Ocul Surf 6 : 117—127, 2008.
60) **Ramos JL, Li Y, Huang D** : Clinical and research applications of anterior segment optical coherence tomography-a review. Clin Experiment Ophthalmol 37 : 81—89, 2009.
61) **Akiba M, Maeda N, Yumikake K, Soma T, Nishida K, Tano Y,** et al : Ultrahigh-resolution imaging of human donor cornea using full-field optical coherence tomography. J Biomed Opt 12 : 041202, 2007.
62) **Maeda N** : Optical coherence tomography for corneal diseases. Eye & Contact Lens 5 : 254—259, 2010.
63) **Grieve K, Paques M, Dubois A, Sahel J, Boccara C, Le Gargasson JF** : Ocular tissue imaging using ultrahigh-resolution, full-field optical coherence tomography. Invest Ophthalmol Vis Sci 45 : 4126—4131, 2004.
64) **Grieve K, Dubois A, Simonutti M, Paques M, Sahel J, Le Gargasson JF,** et al : *In vivo* anterior segment imaging in the rat eye with high speed white light full-field optical coherence tomography. Opt Express 13 : 6286—95, 2005.
65) **Akiba M, Chan KP** : *In vivo* video-rate cellular-level full-field optical coherence tomography. J Biomed Opt 12 : 064024, 2007.
66) **Kawana K, Kiuchi T, Yasuno Y, Oshika T** : Evaluation of trabeculectomy blebs using 3-dimensional cornea and anterior segment optical coherence tomography. Ophthalmology 116 : 848—855, 2009.
67) **Kymionis GD, Suh LH, Dubovy SR, Yoo SH** : Diagnosis of residual Descemet's membrane after Descemet's stripping endothelial keratoplasty with anterior segment optical coherence tomography. J Cataract Refract Surg 32 : 1827—1835, 2006.
68) **Li Y, Meisler DM, Tang M, Lu AT, Thakrar V, Reiser BJ,** et al : Keratoconus diagnosis with optical coherence tomography pachymetry mapping. Ophthalmology 115 : 2159—2166, 2008.
69) **Stahl JE, Durrie DS, Schwendeman FJ, Boghossian AJ** : Anterior segment OCT analysis of thin IntraLase femtosecond flaps. J Refract Surg 23 : 555—558, 2007.
70) **von Jagow B, Kohnen T** : Corneal architecture of femtosecond laser and microkeratome flaps imaged by anterior segment optical coherence tomography. J Cataract Refract Surg 35 : 35—41, 2009.
71) **Lim LS, Aung HT, Aung T, Tan DT** : Corneal imaging with anterior segment optical coherence tomography for lamellar keratoplasty procedures. Am J Ophthalmol 145 : 81—90, 2008.
72) **Holz HA, Meyer JJ, Espandar L, Tabin GC, Mifflin MD, Moshirfar M** : Corneal profile analysis after Descemet stripping endothelial keratoplasty and its relationship to postoperative hyperopic shift. J Cataract Refract Surg 4 : 211—214, 2008.
73) **Lombardo M, Terry MA, Lombardo G, Boozer DD, Serrao S, Ducoli P** : Analysis of posterior donor corneal parameters 1 year after Descemet stripping automated endothelial keratoplasty (DSAEK) triple procedure. Graefes Arch Clin Exp Ophthalmol 248 : 421—427, 2010.
74) **Miura M, Mori H, Watanabe Y, Usui M, Kawana K, Oshika T,** et al : Three-dimensional optical coherence tomography of granular corneal dystrophy. Cornea 26 : 373—374, 2007.
75) **Mori H, Miura M, Iwasaki T, Goto H, Sakurai Y, Watanabe Y,** et al : Three-dimensional optical coherence tomography-guided phototherapeutic keratectomy for granular corneal dystrophy. Cornea 28 : 944—947, 2009.
76) **Yasuno Y, Madjarova VD, Makita S, Akiba M, Morosawa A, Chong C,** et al : Three-dimensional and high-speed swept-source optical coherence tomography for *in vivo* investigation of human anterior eye segments. Opt Express 13 : 10652—10664, 2005.

Biomaterials 32 (2011) 3358–3366

Contents lists available at ScienceDirect

Biomaterials

journal homepage: www.elsevier.com/locate/biomaterials

Transparent, tough collagen laminates prepared by oriented flow casting, multi-cyclic vitrification and chemical cross-linking

Yuji Tanaka [a,b], Koichi Baba [c,d], Thomas J. Duncan [a,e], Akira Kubota [a], Toru Asahi [f], Andrew J. Quantock [e], Masayuki Yamato [b], Teruo Okano [b], Kohji Nishida [a,c,d,*]

[a] Department of Ophthalmology and Visual Science, Tohoku University Graduate School of Medicine, 1-1 Seiryo-machi, Aoba-ku, Sendai, Miyagi 980-8574, Japan
[b] Institute of Advanced Biomedical Engineering and Science, Tokyo Women's Medical University, TWIns, 8-1 Kawada-cho, Shinjuku-ku, Tokyo 162-8666, Japan
[c] Advanced Ophthalmic Medicine, Tohoku University Graduate School of Medicine, 1-1 Seiryo-machi, Aoba-ku, Sendai, Miyagi 980-8574, Japan
[d] Department of Ophthalmology, Osaka University Medical School, Yamadaoka 2–2, Suita, Osaka 565–0871, Japan
[e] Structural Biophysics Group, School of Optometry and Vision Sciences, Cardiff University, Maindy Road, Cardiff CF24 4LU, Wales, UK
[f] Consolidated Research Institute for Advanced Science and Medical Care, Waseda University, 513 Wasedatsurumaki-cho, Shinjuku-ku, Tokyo, 162-0041, Japan

ARTICLE INFO

Article history:
Received 12 September 2010
Accepted 6 November 2010
Available online 5 February 2011

Keywords:
Collagen structure
Biomimetic material
Fibrous tissue
Biofilm
Soft tissue biomechanics
Cornea

ABSTRACT

The lamellar architecture found in many natural fibrous tissues has a significant bearing on their specific functions. However, current engineered tissues have simultaneously no realistic structures and no adequate functions. This study demonstrates a two-step process for obtaining structurally mimicking laminates in natural fibrous tissues with good optical and mechanical characters from purified-clinically-safe collagen molecules. Stacked lamella structures can be created by repeating flow casting, with the controlling parallel/orthogonal directionalities of each thin single-layer (2–5 μm in thickness). The transparency of laminates is successfully improved by a unique multi-cyclic vitrification with chemical cross-linking. The directionalities of optical and mechanical functions in laminates are strongly related with the preferential collagen alignments in the laminates. The tensile strength of laminates is extremely higher than any other engineered materials as well as native cornea, which exhibit an orthogonal laminated collagen structure and a good optical transmission.

1. Introduction

Engineering of nano/micro-structures having specific functions have attracted attention in the field of material science, and it's one of the key topics for tissue regeneration [1]. In mammals, collagen is the most abundant protein where it gives the primary structural component of extracellular matrix [2,3]. The hierarchical molecular, fibrillar, and supra-fibrillar architecture of collagen has a huge bearing on tissue functions [1,4,5]. A highly illustrative example is the cornea in which collagen molecules self-assemble into remarkably uniform thin fibrils with approx. 31 nm diameter and aligns themselves into a stacked orthogonal lamellar array with approx. 500 μm thick and 200-300 lamellae in humans [6–9]. Its short-range spatial order in lateral arrangement permits high transparency, [8,10,11] and their axial alignments that point to ocular muscles, might import mechanical strength to the cornea [12–17]. Similar lamellar architectures are also found in other collagen-rich fibrocartilages such as bone, [5] meniscus, [18] and intervertebral disc, [19] which require much stronger mechanical tolerance with directionalities. However, such structures and functions in fibrous tissues are unable to be recovered naturally from severe injuries and diseases, and current cell-culture-based regenerative medicine [20–22] is inefficient. Therefore, it is necessary to engineer functionally suitable fibrous tissue replacements by material-based approaches for providing curative treatments that replace conventional palliative cares [1].

Fibrous tissue engineering from purified collagen molecules was firstly reported over 30 years ago [23]. Subsequently reconstructions of full-thickness skin, [24] blood vessels, [25,26] and corneas [27–30] have been reported, but such current studies are still in their infancy. There are a few researches especially for mechanical regeneration, [1,31,32] although collagen alignments can be achieved by applying strong magnetic fields, [33,34] electron spinning, [35,36] dip pen nanolithography, [37] self-assembly, [38] patterned surfaces, [2] and flow manipulations [39–41]. Recently, our group revealed that the mechanical anisotropy of thick (0.4–1.2 mm) collagen mono-layers links with molecular directionality induced by extensional flow [31,32]. Nerurkar NL et al demonstrated a mechanical improvement by creating thick angle-ply bi-lamellar

* Corresponding author. Department of Ophthalmology, Osaka University Medical School, Yamadaoka 2–2, Suita 565–0871, Japan. Tel.: +81 6 6879 3450/3451; fax: +81 6 6879 3459.
E-mail address: knishida@ophthal.med.osaka-u.ac.jp (K. Nishida).

0142-9612/$ – see front matter © 2010 Elsevier Ltd. All rights reserved.
doi:10.1016/j.biomaterials.2010.11.011

structures with mesenchymal stem cells (MSC) by electron spinning [1]. These works well indicate the importance of nano/microstructural mimicking for obtaining the adequate mechanical strength, but they are unable to completely mimic natural tissues, particularly in the number of lamella and their thickness. On the other hand, the optical regeneration of cornea have been examined by cross-linking collagen molecules dissolved in acidic solution, [30–32,42] proteoglycan conjugation, [34] and dehydration at low temperature (vitrification), [43,44] but such transparent constructs have simultaneously no realistic structures (i.e. microfibrils, alignments, and lamella structures) and no adequate mechanical functions. Thus, the next challenge in this field will be the development of structurally mimicking laminate structures with good mechanical and optical functions, particularly for cornea.

Here, a two-step process is proposed to prepare parallel and orthogonal laminates with both transparency and rigidity from a pepsin-treated collagen (Atelocollagen), which exhibits a good biocompatibility for clinical use [28–32,42,45,46]. As a first step, an oriented flow casting system and vitrification were applied for laminating fine collagen layers with thinner thickness (<10 μm). As a second step, a unique multi-cyclic vitrification [43,44,47] with chemical cross-linking was adopted for improving their transparency stably. The obtained transparent stacked collagen laminates were characterized structurally and functionally (optics and mechanics) by focusing on their relationships.

2. Materials and methods

2.1. Preparation of collagen laminates with a specific alignment by simple flow casting

Flow casting of 3% atelocollagen (Atelocollagen Implant) (Koken, Tokyo, Japan) was done on a tilted cover glass (24 × 32 mm) on a handcrafted stage with a swing type centrifugation machine. The spread wet collagen layer on the cover glass was incubated at 37 °C for 30 min and put a cold room until the layer was dried. Subsequent parallel or orthogonal flow casting was performed on a dry collagen layer that was rotated by 180° or 90°, and the incubation and dry treatment were repeated as the first layer. These processes were repeated for laminating collagen layers.

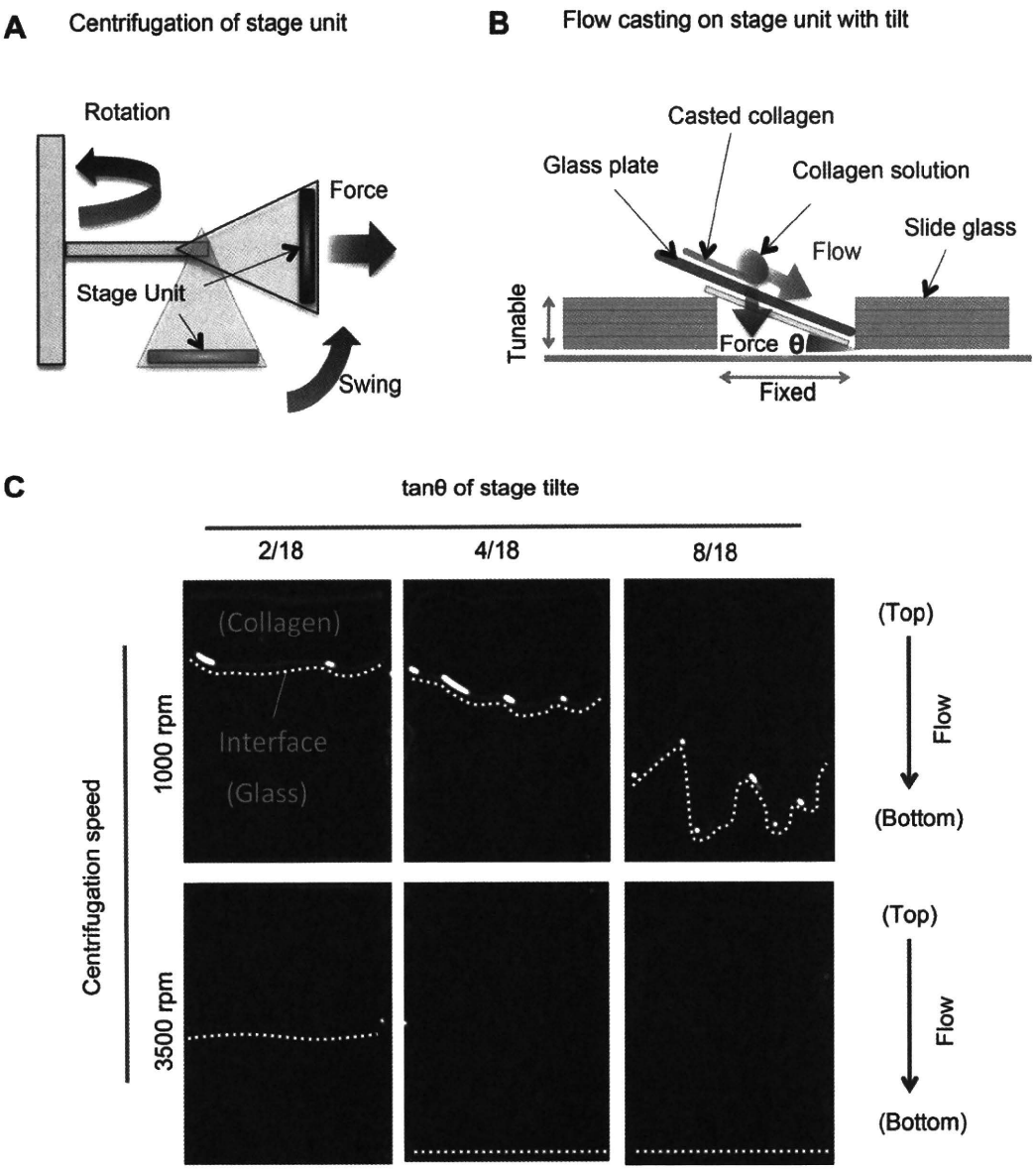

Fig. 1. (A, B) Scheme of a method for creating thin collagen layer by flow casting with directionalities. (A) Centrifugation of stage unit with a typical swing type apparatus; (B) The flow casting of collagen on stage unit with tilted glass plate. (C) The photographs of spread collagen solutions on glass plates at various tilte angles and centrifugation speeds for optimizing flow casting.

2.2. Multi-cyclic optical clearing of collagen laminates and visible-light transmission analysis

Collagen laminates obtained by flow casting were treated by multi-cyclic vitrification with chemical cross-linking. Briefly, dried collagen laminates were cross-linked with a mixture of EDC (Wako pure chemicals, Osaka, Japan) and NHS (Thermo science, Rockford, IL, USA) (the molecular ratio of EDC/NHS :2/1) at room temperature for 2 h. These cross-linking reagents were washed out with natural saline and distilled water, subsequently the samples were dried at low temperature at 4–8 °C. Repetition of the low-temperature drying, cross-linking, and washing processes were quantitatively evaluated by visible-light transmission measurements.

2.3. Polarizing light microscope imaging

For cross-section analysis, 200-μm-thick cross-sections were created by sectioning the frozen block of laminates with cryostat. The sections of samples were placed on the slide glass, washed with distilled water, covered with a cover glass with Dulbecco's phosphate buffered saline (PBS), and analyzed by a polarizing light microscope with λ plate (DMLB-S) (Leica, Ppstach, Germany). Angles of polarizer and analyzer were set at −45° and +45° from the direction of analysts surface. For flat-mount analysis, collagen laminates were put on glass slide and observed under a polarizing light microscope. Angles of polarizer and analyzer were set at 0° and +90°, and the flow axis of sample's first layer was rotated for 4 times by 45° from 0°, which parallel to the polarizer.

2.4. SEM imaging

Cross-sections of collagen laminates were prepared by cutting the sample in direction parallel and perpendicularly to the flow. Critical point dry was performed with a critical point dryer (HCP-2) (Hitachi, Hitachi, Japan) with carbon dioxide, after pretreatment with elevated ethanol and isoamyl acetete. The cross-sections of the prepared dried tissues were coated with osmium with an osmium coater (HPC-30) (Vacuum Device, Ibaragi, Japan), and observed with SEM (JSM-6700F) (JEOL, Tokyo, Japan).

2.5. TEM imaging

Sections (approximately 2 × 1 mm in size) were cut from samples, fixed with 4% paraformaldehyde followed by 2% osmium textroxide, dehydrated through a graded series of ethanol, embedded in epoxy resin, and cured. Ultrathin sections (70–90 nm in thickness) were cut in a direction parallel and perpendicularly to the flow on an ultramicrotome, placed on TEM grids, and stained at room temperature with 2% uranyl acetate, 1% PTA and reynolds lead citrate. Collagen laminates were imaged with a TEM (Hitachi H-7600) (Hitachi, Hitachi, Japan).

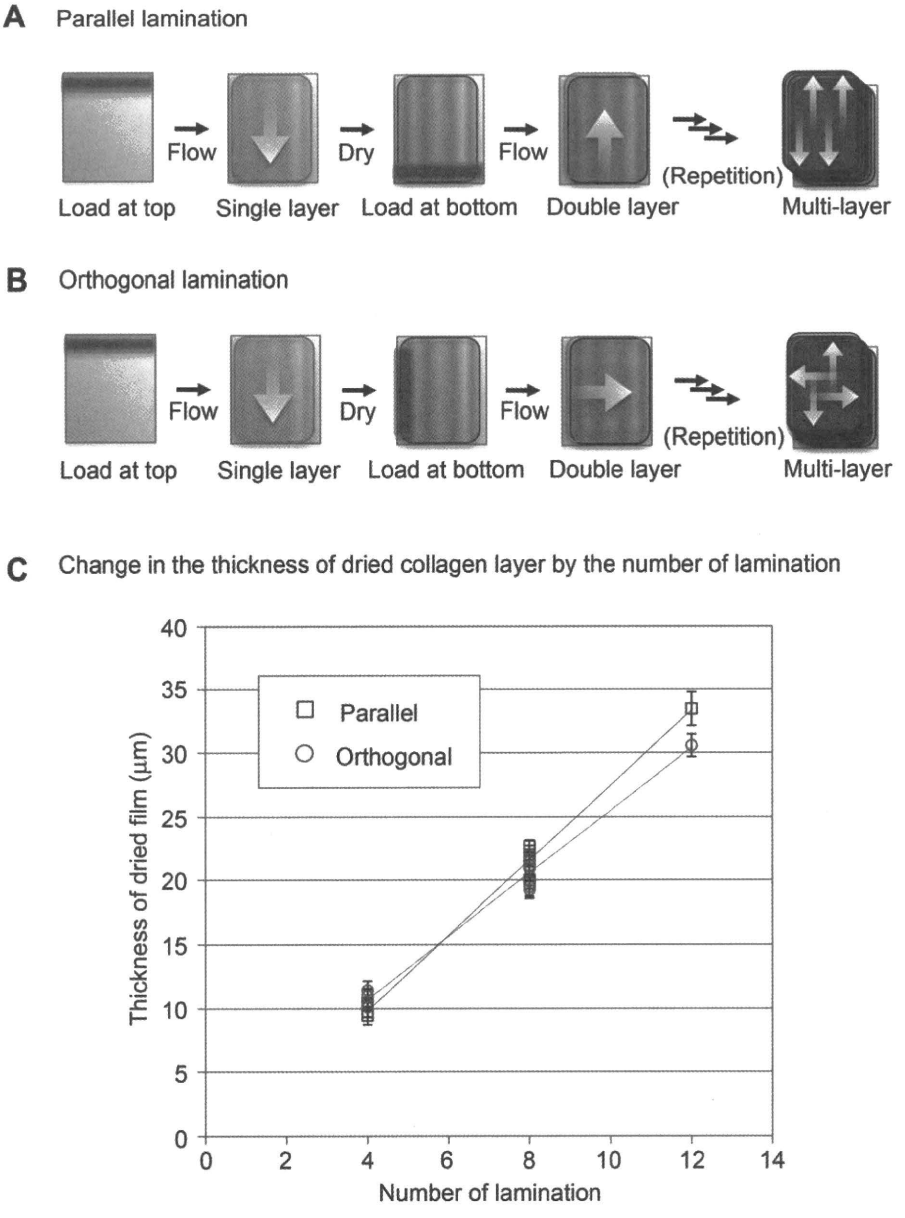

Fig. 2. (A, B) Scheme of lamination with rotating directionality upon flow casting. (A) Parallel lamination;(B) orthogonal lamination.(C) Change in the thickness of dry collagen laminate by repeating parallel and orthogonal lamination by flow casting.

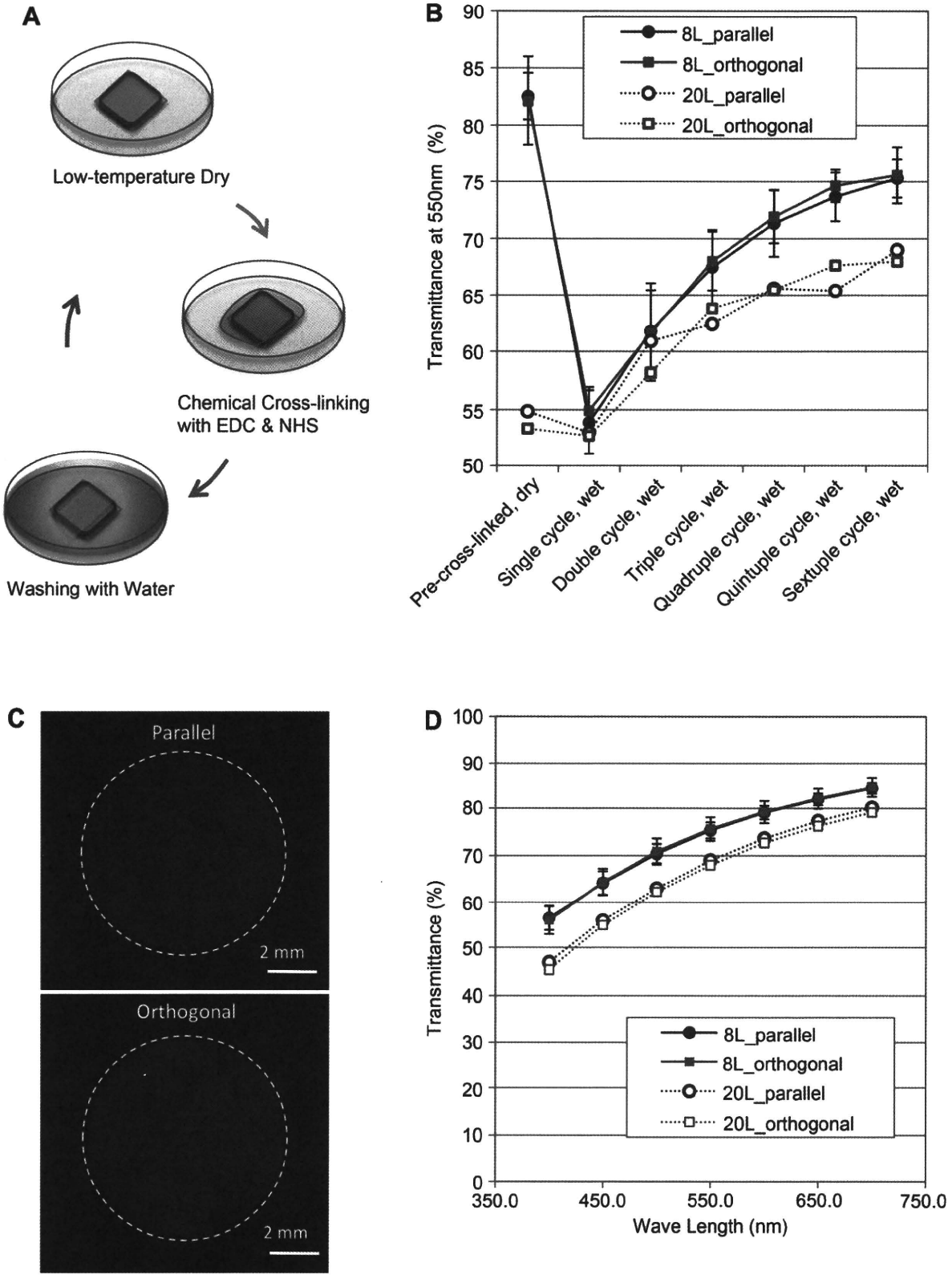

Fig. 3. (A) Scheme of multi-cyclic optical clearing of collagen laminates by low-temperature-dry and chemical cross-linking. (B) Improvement of light transmission of 8-layered (8L) collagen laminates and 20-layered (20L) collagen laminates by increasing the cycle number of optical clearing (mean ± SD, $n = 6$, in the case of 8L collagen laminates). (C) photographs of 8-mm-trephined 20L collagen laminates in Dulbecco's phosphate buffered Saline (PBS) after sextuple-cycle optical clearing. (D) The visible-light transmission of the obtained 8L and 20L collagen laminates in PBS after sextuple-cycle optical clearing (mean ± SD, $n = 6$, in the case of 8L collagen laminates).

2.6. Mechanical testing

Tensile strength of PBS-containing collagen laminates were measured with a Table-Top Universal Testing Instruments (EZ Test) (Shimadzu, Kyoto, Japan) at a rate of 100 mm/min, after molding into a dumbbell-shape to enhance the gripping of the holding fixture and prevent rupture at the fixture. The region under measurement was rectangular in shape (10 mm in length, 3 mm in width, and 400 μm in thickness) parallel to and perpendicularly to the direction of flow. The stress was monitored as a function of strain, and the elastic modulus was obtained by calculating the slope of the linear region in the resulting stress-strain curves.

3. Results and discussion

3.1. Lamination of collagen by oriented flow casting

For laminating fibrous type I atelocollagen with strictly regulated thickness and directionalities, an oriented flow casting method was firstly developed by modifying swing type centrifugation (Fig. 1). Directionality of flow was able to be controlled

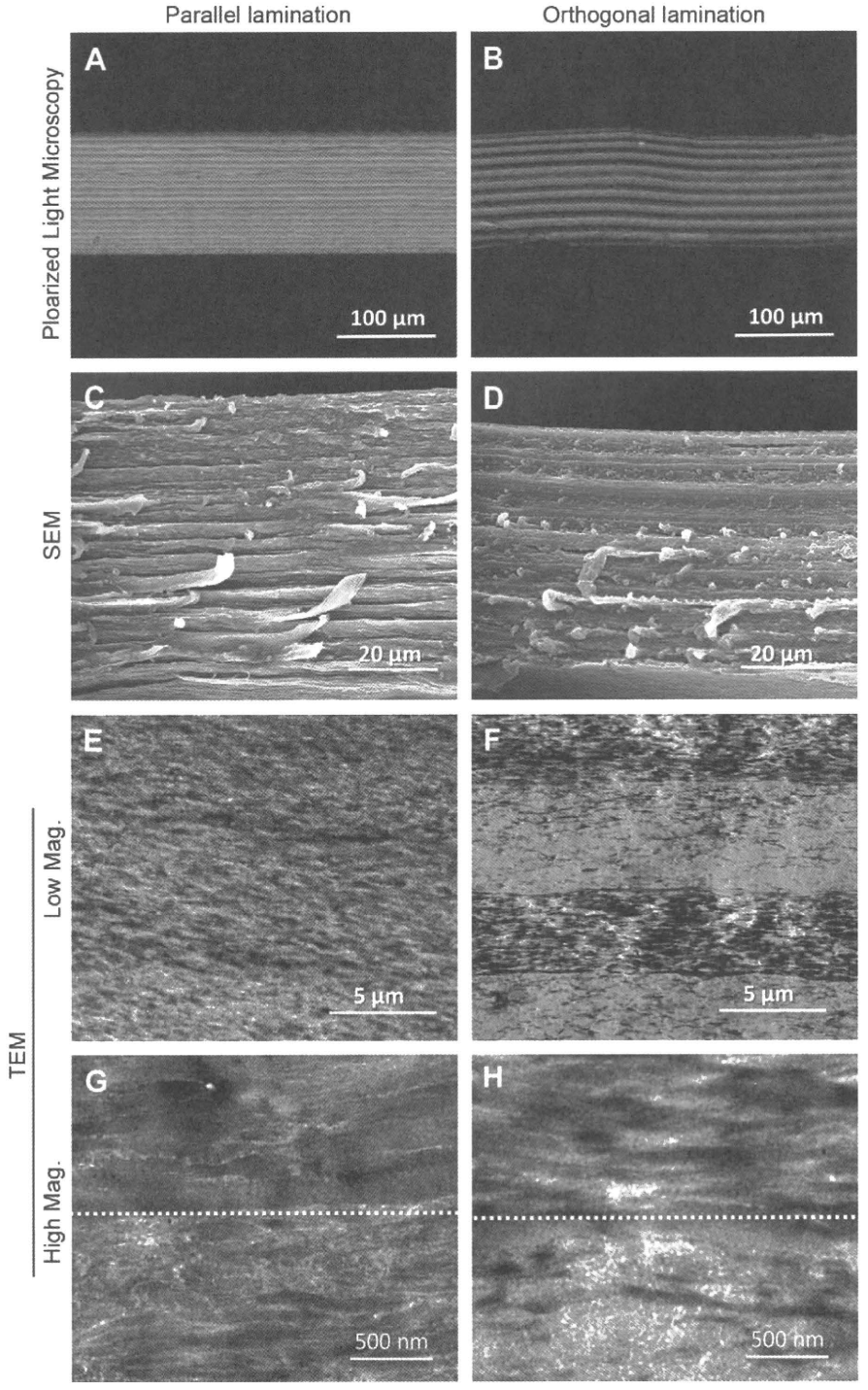

Fig. 4. Structural characterization of 20-layered collagen laminates which treated after sextuple-cycle optical clearing. Cross-section of collagen laminates with parallel (A, C, E, and E) and orthogonal (B, D, F, and H) directionalities. (A, B) Polarizing light microscope imaging of frozen section; c) and d) SEM imaging of cross-section created with a blade; (E, F) TEM imaging of ultrathin section at low magnification;(G, H) TEM imaging at high magnification. All cross-sections were prepared parallel to the flow direction of first layer. Dashed lines represent interface of two layers.

by centrifuging a tilted flat glass surface (Fig. 1A and B). Wider spreading areas of collagen solution on glass plate were achieved at higher centrifugation speed and larger tilt angle at 4 °C (Fig. 1C). A wet collagen layer on glass plate was incubated at 37 °C and vitrified at 4–8 °C for creating a rigid collagen films. The thickness of the dry monolayer on a glass plate was uniformly regulated to be 4.3 μm and 2.3 μm at any position by tangent θ (the tilt angle) of 4/18 and 8/18 at a centrifugation rotation speed of 3500 rpm, respectively (the second row and the middle column, and the second raw and the right column, Fig. 1C). They are extremely thinner than previous studies such as our single-layer by extensional flow [31,32] and, orthogonal tri-laminate by magnetic alignment, [34] and angle-ply bi-laminate with MSC by electron spinning [1].

Subsequent parallel or orthogonal flow casting was performed on a dry collagen layer that was rotated by 180° (Fig. 2A) or 90° (Fig. 2B), and these procedures were repeated. The repetition of this lamination process was unable to be achieved without preparing rigid collagen layers by both pre-incubation and vitrification. The pre-incubation before drying was essential for generating a smoother and clearer macroscopic surface morphology with thicker microfiber-like structures (Supporting Information 1), which seems to be linked with collagen fibrogenesis. Vitrification is also reported to reduce thickness as well as giving better transparency [43]. The thickness of the dry laminate was proportional to the number of repetitions of the flow casting procedure, and the calculated thickness of each layer was regulated to be less than 3 μm (Fig. 2C). Increase in number of collage lamella is not easily achieved by other methods, and they are less than 10 layers [1,34]. However, the lamination process, proposed by this study (Figs. 1 and 2), was confirmed to be able to be repeated at least 20 times without substantial change in the smoothness or rigidity of dry laminate surface.

3.2. Cyclic vitrification with chemical cross-linking for optical clearing of laminates and evaluation of transparency

Although structural and functional stabilities at wet condition should be considered upon the clinical application of the collagen laminates, the obtained laminates by our method were significantly swelled by rehydration with loosing their transparency and mechanical rigidity. For avoiding these unwelcome characters, this study used chemical cross-linking method with ethylenedichloride (EDC) and N-hydroxy succinimide (NHS) (EDC/NHS), which is better biocompatibility than other chemical crosslinkers [4,31,42]. The method was confirmed to inhibit the swelling of collagen layer at wet conditions and to increase the mechanical strength by promoting inter-fiber chemical bonding [4,31,32,42]. Furthermore, a unique repetition process for optical clearing by vitrification with chemical cross-linking was also investigated (Fig. 3A), because single cross-linking treatment was imperfect for obtaining transparency (lower than 55% at 550 nm) (Fig. 3B, single cycle). Interestingly, this repetition strategy monotonically improved the transparency of both 8-layered and 20-layered laminates at wet condition up to 75% and 68% at 550 nm, respectively (Fig. 3B), and the high transparency of the products were realized by naked eye inspection (Fig. 3C). Their visible-light transmissions improved with increasing wavelength with no significant difference between their laminating directionalities, parallel flow and orthogonal flow castings (Fig. 3D). The transparency is near the human cornea and higher than both the isolated donor cornea and the amniotic membrane, which widely utilized as an implant for ocular surface treatments [30,48]. In addition, this optical clearing by vitrification with cross-linking could be applicable to the optical clearing of scleral coat, which is white collagen-rich membrane next to the cornea, but repetition of this treatment was inefficient, [49] compared with collagen laminates obtained by this study. The monotonic increase in transparency which found in this study (Fig. 3B) is thought to be derived from fine and regular nano/micro-structural formation in collagen laminates. In addition, the macro-structures of laminates were quite stable during this optical clearing process, and the resultants could be handled by tweezers easily, without any visible break or layer peeling.

3.3. Nano/micro-structural visualization of transparent collagen laminates

To investigate a possible difference in structural architecture between laminating flow directions; parallel, and orthogonal flow castings, the cross-sections of both 20-layered laminates treated by sextet cycle optical clearing were analyzed (Fig. 4). Initially, the directionality of each layer of laminates was observed by polarized light. This type of analysis is often applied for visualizing structural

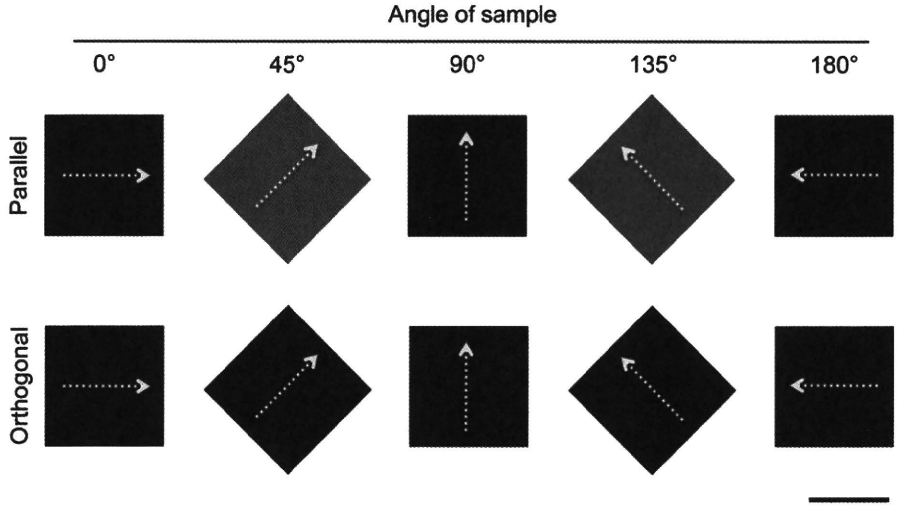

Fig. 5. Polarizing microscopy analysis of flat-mounted parallel and orthogonal 20-layered collagen laminates after sextuple-cycle optical clearing: The flow axis of first layer in each sample was rotated 4 times by 45° from parallel to the polarizer. Scale bar : 500 μm, Lens : 20x, polarizer : 0°, and analyzer : 90°. White arrows represent the directionality of flow applied on the first layer of each laminate.

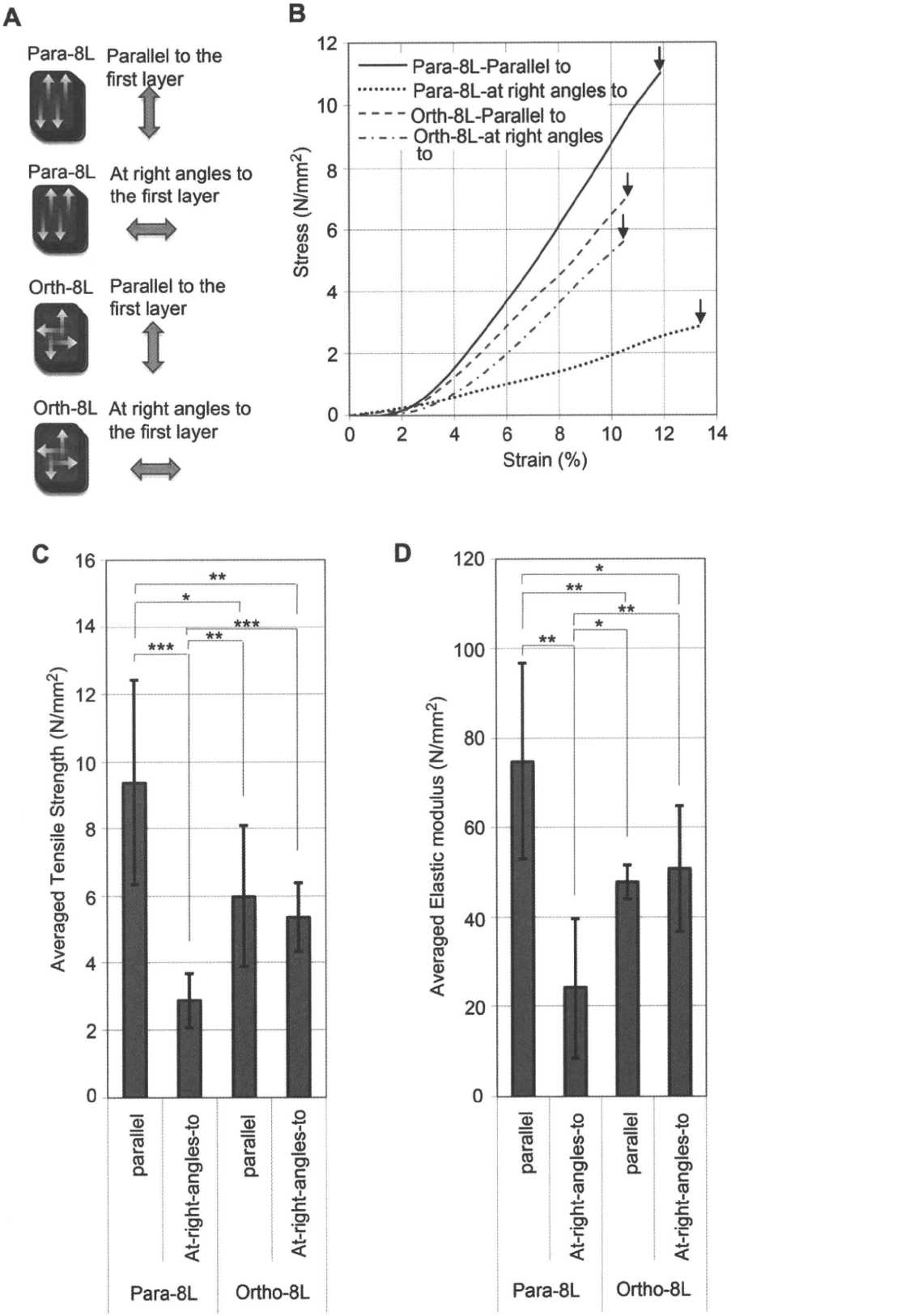

Fig. 6. Mechanical anisotropy evaluation of parallelly and orthogonally laminates in the direction parallel and at right angles to the initial flow. (A) Directionalities of applied tensile stress parallelley and orthogonally to 8-layered (8L) laminates. Yellow arrows indicate the directionalities of applied flow casting. Red arrows indicate the directionality of applied force.(B) Typical stress-strain curves. Black arrows indicate the point of breaking. (C) Comparison of averaged tensile strength (mean ± SD, $n = 7$, $^*P < 0.05$, $^*P < 0.01$, and $^*P < 0.001$). (D) Comparison of averaged elastic modulus (mean ± SD, $n = 7$, $^*P < 0.05$, $^*P < 0.01$, and $^*P < 0.001$).

difference in domains which organize transparent liquid crystalline hydrogels, by detecting the birefringence of the samples [4,31,50]. Bright uniform optical rotation was found from all laminated layers with parallel flows only by an observation direction parallel to the flow (Fig. 4A) (but no bright stripe was observed by an observation direction perpendicular to the flow) (Supporting Information 2). In contrast, bright and dark stripes were alternatively observed on orthogonally flow lamination (Fig. 4B). The surface morphology of cross-section of parallel flow laminates showed a quite fine structure with linear fibrous shapes along flow direction (Fig. 4C), but that of orthogonal flow laminate exhibits a rounded dot-like structure with linear fibrous shapes (Fig. 4D). TEM ultrastructural analysis showed a clear difference in microfiber structure between laminates made by parallel flow (Fig. 4E) and orthogonal flow (Fig. 4F). The highly magnified images of the layer–layer interface of both laminates cleared up their directionality and the morphology of microfiber like collagen with thin diameter (less than approx. 200 nm) (Fig. 4G and H). All of these data strongly supported the achievement of strict regulation of collagen directionalities parallel to the flow cast, which was similar to polymer alignments induced by other flow systems [31,32,39–41,50–52]. And the partial mixture of fibrils between layers with different directionalities was observed at the interface of orthogonal laminates (Fig. 4F), which might contribute the mechanical stability at interface of layers.

3.4. Polarized light transmission analysis through flat-mounted collagen laminates

For revealing the contribution of such structural difference to tissue functions, polarized lights vertically passing through the flat-mounted transparent laminates were additionally observed under a polarized microscopy with a polarizer and analyzer set in orthogonal directionalities (Fig. 5). Darkness was ascertained from both laminates when the flow axis of their first layer is parallel to the polarizer or analyzer (0°, 90°, and 180° to the horizontal axis, the 1st, 3rd, and 5th column, respectively, Fig. 5). But, bright birefringence was observed specifically on the parallel laminate when the sample angle was between 0° and 90°, and 90° and 180°, and the brightness reached their maximum at 45° and 135° (the 2nd and 4th column, Fig. 5). This optical rotation observed on the parallel laminate created by uniaxial flow was similar to the previous our results that observed on the non-laminated thick collagen hydrogels by uniaxial extensional flow [31]. On the other hand, the orthogonal laminate, which is similar structure with the central part of corneal stroma, [6–9] cancelled the transmission of polarized light at any angles (the 2nd row, Fig. 5). Corneal stroma may equip such an isotropic function to cancel the optical rotation of the polarized lights.

3.5. Mechanical characterization of transparent collagen laminates

To verify that parallel and orthogonal lamellar collagen architecture gives difference in macro-mechanical properties, the tensile strength of both parallel and orthogonal 8-layered laminates was measured in the flow axis and antiflow axis of the first layer direction (Fig. 6A). Typically, parallel laminates exhibited steeper stress-strain curves in a parallel direction compared to the anti-axis direction, in contrast, orthogonal laminates exhibit curves similar to that of parallel laminate in both directions (Fig. 6B). The averaged maximum strength and Young's modulus of parallel laminates in parallel direction were 9.38 N/mm^2 and 74.8 N/mm^2, respectively. Those of the orthogonal laminates were 5.98 N/mm^2 and 47.8 N/mm^2 in parallel to the first layer, 5.35 N/mm^2 and 50.7 N/mm^2 orthogonal to the first layer were approximately three-fold higher and two-fold higher than those of parallel laminates in the anti-axis direction (2.86 N/mm^2 and 24.1 N/mm^2), respectively (Fig. 6C and D). These results clearly revealed that the mechanical directionalities were strongly linked with their nano/microscopic fibrous directionalities in laminates. The mechanical anisotropy of parallel laminates found in this study well mimic the tendency found in bone [5]. To our knowledge, all of these mechanical data were higher than those of any other collagen tissue such as transparent cross-linked gels with various additives, [53] anisotropic transparent mono-layers, [31,32] cyclically loaded scaffold, [54]and bi-lamellar constructs with MSC [1]. Furthermore, our orthogonal laminates exhibited an extremely higher mechanical toughness than that of isolated human cornea (3.81 N/mm^2 tensile at break and3-13 N/mm^2 in modulus) [12,13]. Thus, the mechanical stability (or rigidity) of the laminates prepared by this study is considered to be closely applicable as fibrous tissue replacements in medical practice.

4. Conclusions

In summary, this study developed a unique and mass production-friendly two-step process for obtaining transparent and tough fibrous collagen laminates, which demonstrated their superb optical and mechanical characters better than those of materials made by conventional methods. The preferential alignments regulated by oriented flow casting significantly affected the transmission of polarized lights and the directionalities of mechanical properties. In addition, an optical clearing with vitrification and cross-linking improved the visible-light transmission effectively. This study can provide a strategy for the reconstruction of nano/microscopic structures and their optical/mechanical characters found in native fibrous tissues. These finding will be important in the field of material science and beneficial for tissue engineering and regenerative medicine, particularly for ocular treatments.

Acknowledgements

The authors are grateful to Mr. T. Suzuki, Waseda University for their kind help regarding polarized microscopy, Dr. K. Fukumori, Tokyo Women's Medical University (TWIns) for his help of surface analysis, and Dr. S. Dong and Miss Y. Sasaki, Tohoku University for their helpful support. This work was financially supported by the Health and Labor Sciences Research Grants of Japan at Tohoku University, Tohoku University Global COE for conquest of Signal Transduction Disease with "Network Medicine" from the Ministry of Education, Culture, Sports, Science and Technology (MEXT), Japan, Tokyo Women's Medical University Formation of Innovation Center for Fusion of Advanced Technologies in the Special Coordination Funds for Promoting Science and Technology from MEXT, Japan, and the EPSRC grant at Cardiff University.

Appendix

Figures with essential color discrimination. Figs. 1–3 and 6 in this article are difficult to interpret in black and white. The full color images can be found in the online version, at doi:10.1016/j.biomaterials.2010.11.011.

Appendix. Supplementary data

Supplementary data associated with this article can be found in the online version, at doi:10.1016/j.biomaterials.2010.11.011.

References

[1] Nerurkar NL, Baker BM, Sen S, Wible EE, Elliott DM, Mauck RL. Nanofibrous biologic laminates replicate the form and function of the annulus fibrosus. Nat Mater 2009;8(12):986–92.

[2] Denis FA, Pallandre A, Nysten B, Jonas AM, Dupont-Gillain CC. Alignment and assembly of adsorbed collagen molecules induced by anisotropic chemical nanopatterns. Small 2005;1(10):984–91.

[3] Di Lullo GA, Sweeney SM, Korkko J, Ala-Kokko L, San Antonio JD. Mapping the ligand-binding sites and disease-associated mutations on the most abundant protein in the human, type I collagen. J Biol Chem 2002;277(6): 4223–31.

[4] Knight DP, Nash L, Hu XW, Haffegee J, Ho MW. In vitro formation by reverse dialysis of collagen gels containing highly oriented arrays of fibrils. J Biomed Mater Res 1998;41(2):185–91.

[5] Seto J, Gupta HS, Zaslansky P, Wagner HD, Fratzl P. Tough lessons from bone: extreme mechanical anisotropy at the mesoscale. Adv Funct Mater 2008;18 (13):1905–11.

[6] Birk DE. Type V collagen: heterotypic type I/V collagen interactions in the regulation of fibril assembly. Micron 2001;32(3):223–37.

[7] Holmes DF, Gilpin CJ, Baldock C, Ziese U, Koster AJ, Kadler KE. Corneal collagen fibril structure in three dimensions: structural insights into fibril assembly, mechanical properties, and tissue organization. Proc Natl Acad Sci USA 2001;98(13):7307–12.

[8] Maurice DM. The structure and transparency of the cornea. J Physiol 1957;136 (2):263–86.

[9] Meek KM, Fullwood NJ. Corneal and scleral collagens–a microscopist's perspective. Micron 2001;32(3):261–72.

[10] Freund DE, McCally RL, Farrell RA. Direct summation of fields for light scattering by fibrils with applications to normal corneas. Appl Opt 1986;25 (16):2739.

[11] Doutch J, Quantock AJ, Smith VA, Meek KM. Light transmission in the human cornea as a function of position across the ocular surface: theoretical and experimental aspects. Biophys J 2008;95(11):5092–9.

[12] Boote C, Dennis S, Huang Y, Quantock AJ, Meek KM. Lamellar orientation in human cornea in relation to mechanical properties. J Struct Biol 2005;149 (1):1–6.

[13] Hayes S, Boote C, Lewis J, Sheppard J, Abahussin M, Quantock AJ, et al. Comparative study of fibrillar collagen arrangement in the corneas of primates and other mammals. Anat Rec (Hoboken) 2007;290(12):1542–50.

[14] Franchi M, Trire A, Quaranta M, Orsini E, Ottani V. Collagen structure of tendon relates to function. Scientific World J 2007;7:404–20.

[15] Thomopoulos S, Marquez JP, Weinberger B, Birman V, Genin GM. Collagen fiber orientation at the tendon to bone insertion and its influence on stress concentrations. J Biomech 2006;39(10):1842–51.

[16] Silver FH, Freeman JW, Seehra GP. Collagen self-assembly and the development of tendon mechanical properties. J Biomech 2003;36(10):1529–53.

[17] Sasaki N, Odajima S. Stress–strain curve and Young's modulus of a collagen molecule as determined by the X-ray diffraction technique. J Biomech 1996;29(5):655–8.

[18] Petersen W, Tillmann B. Collagenous fibril texture of the human knee joint menisci. Anat Embryol (Berl) 1998;197(4):317–24.

[19] Iatridis JC, ap Gwynn I. Mechanisms for mechanical damage in the intervertebral disc annulus fibrosus. J Biomech 2004;37(8):1165–75.

[20] Rama P, Matuska S, Paganoni G, Spinelli A, De Luca M, Pellegrini G. Limbal stem-cell therapy and long-term corneal regeneration. N Engl J Med 2010;363 (2):147–55.

[21] Nishida K, Yamato M, Hayashida Y, Watanabe K, Yamamoto K, Adachi E, et al. Corneal reconstruction with tissue-engineered cell sheets composed of autologous oral mucosal epithelium. N Engl J Med 2004;351(12):1187–96.

[22] Hsieh MM, Kang EM, Fitzhugh CD, Link MB, Bolan CD, Kurlander R, et al. Allogeneic hematopoietic stem-cell transplantation for sickle cell disease. N Engl J Med 2009;361(24):2309–17.

[23] Bell E, Ivarsson B, Merrill C. Production of a tissue-like structure by contraction of collagen lattices by human fibroblasts of different proliferative potential in vitro. Proc Natl Acad Sci USA 1979;76(3):1274–8.

[24] Bell E, Ehrlich HP, Buttle DJ, Nakatsuji T. Living tissue formed in vitro and accepted as skin-equivalent tissue of full thickness. Science 1981;211 (4486):1052–4.

[25] L'Heureux N, Dusserre N, Konig G, Victor B, Keire P, Wight TN, et al. Human tissue-engineered blood vessels for adult arterial revascularization. Nat Med 2006;12(3):361–5.

[26] L'Heureux N, Paquet S, Labbe R, Germain L, Auger FA. A completely biological tissue-engineered human blood vessel. FASEB J 1998;12(1):47–56.

[27] Griffith M, Osborne R, Munger R, Xiong X, Doillon CJ, Laycock NL, et al. Functional human corneal equivalents constructed from cell lines. Science 1999;286(5447):2169–72.

[28] Liu L, Kuffova L, Griffith M, Dang Z, Muckersie E, Liu Y, et al. Immunological responses in mice to full-thickness corneal grafts engineered from porcine collagen. Biomaterials 2007;28(26):3807–14.

[29] Liu W, Merrett K, Griffith M, Fagerholm P, Dravida S, Heyne B, et al. Recombinant human collagen for tissue engineered corneal substitutes. Biomaterials 2008;29(9):1147–58.

[30] Liu Y, Gan L, Carlsson DJ, Fagerholm P, Lagali N, Watsky MA, et al. A simple, cross-linked collagen tissue substitute for corneal implantation. Invest Ophthalmol Vis Sci 2006;47(5):1869–75.

[31] Tanaka Y, Kubota A, Matsusaki M, Duncan T, Hatakeyama Y, Fukuyama K, et al. Anisotropic mechanical properties of collagen hydrogels induced by uniaxial-flow for ocular applications. J Biomater Sci Polym Ed; 2010 [Epub ahead of print].

[32] Duncan TJ, Tanaka Y, Shi D, Kubota A, Quantock AJ, Nishida K. Flow-manipulated, crosslinked collagen gels for use as corneal equivalents. Biomaterials 2010;31(34):8996–9005.

[33] Guo C, Kaufman LJ. Flow and magnetic field induced collagen alignment. Biomaterials 2007;28(6):1105–14.

[34] Torbet J, Malbouyres M, Builles N, Justin V, Roulet M, Damour O, et al. Orthogonal scaffold of magnetically aligned collagen lamellae for corneal stroma reconstruction. Biomaterials 2007;28(29):4268–76.

[35] Zhong S, Teo WE, Zhu X, Beuerman RW, Ramakrishna S, Yung LY. An aligned nanofibrous collagen scaffold by electrospinning and its effects on in vitro fibroblast culture. J Biomed Mater Res A 2006;79(3):456–63.

[36] Chew SY, Mi R, Hoke A, Leong KW. Aligned protein-polymer composite fibers enhance nerve regeneration: a potential tissue-engineering platform. Adv Funct Mater 2007;17(8):1288–96.

[37] Wilson DL, Martin R, Hong S, Cronin-Golomb M, Mirkin CA, Kaplan DL. Surface organization and nanopatterning of collagen by dip-pen nanolithography. Proc Natl Acad Sci USA 2001;98(24):13660–4.

[38] Cisneros DA, Friedrichs J, Taubenberger A, Franz CM, Muller DJ. Creating ultrathin nanoscopic collagen matrices for biological and biotechnological applications. Small 2007;3(6):956–63.

[39] Koster S, Leach JB, Struth B, Pfohl T, Wong JY. Visualization of flow-aligned type I collagen self-assembly in tunable pH gradients. Langmuir 2007;23 (2):357–9.

[40] Lanfer B, Freudenberg U, Zimmermann R, Stamov D, Korber V, Werner C. Aligned fibrillar collagen matrices obtained by shear flow deposition. Biomaterials 2008;29(28):3888–95.

[41] Kirkwood JE, Fuller GG. Liquid crystalline collagen: a self-assembled morphology for the orientation of mammalian cells. Langmuir 2009;25(5):3200–6.

[42] Liu Y, Griffith M, Watsky MA, Forrester JV, Kuffova L, Grant D, et al. Properties of porcine and recombinant human collagen matrices for optically clear tissue engineering applications. Biomacromolecules 2006;7(6):1819–28.

[43] Takezawa T, Ozaki K, Nitani A, Takabayashi C, Shimo-Oka T. Collagen vitrigel: a novel scaffold that can facilitate a three-dimensional culture for reconstructing organoids. Cell Transplant 2004;13(4):463–73.

[44] Takezawa T, Ozaki K, Takabayashi C. Reconstruction of a hard connective tissue utilizing a pressed silk sheet and type-I collagen as the scaffold for fibroblasts. Tissue Eng 2007;13(6):1357–66.

[45] Furthmayr H, Timpl R. Immunochemistry of collagens and procollagens. Int Rev Connect Tissue Res 1976;7:61–99.

[46] Ochi M, Uchio Y, Tobita M, Kuriwaka M. Current concepts in tissue engineering technique for repair of cartilage defect. Artif Organs 2001;25(3): 172–9.

[47] Takushi E, Asato L, Nakada T. Edible eyeballs from fish. Nature 1990;345: 298–9.

[48] Connon CJ, Doutch J, Chen B, Hopkinson A, Mehta JS, Nakamura T, et al. The variation in transparency of amniotic membrane used in ocular surface regeneration. Br J Ophthalmol 2009;94:1057–61.

[49] Tanaka Y, Kubota A, Yamato M, Okano T, Nishida K. Irreversible optical clearing of sclera by simple drying and cross-linking. Biomaterials 2011;32 (4):1080–90.

[50] Zhang S, Greenfield MA, Mata A, Palmer LC, Bitton R, Mantei JR, et al. A self-assembly pathway to aligned monodomain gels. Nat Mater 2010;9 (7):594–601.

[51] Bent J, Hutchings LR, Richards RW, Gough T, Spares R, Coates PD, et al. Neutron-mapping polymer flow: scattering, flow visualization, and molecular theory. Science 2003;301(5640):1691–5.

[52] Cheema U, Chuo CB, Sarathchandra P, Nazhat SN, Brown RA. Engineering functional collagen scaffolds by mechanical loading. In: Tissue Engineering 2007;vol. 13(7):1688–1688.

[53] Liu W, Deng C, McLaughlin CR, Fagerholm P, Lagali NS, Heyne B, et al. Collagen-phosphorylcholine interpenetrating network hydrogels as corneal substitutes. Biomaterials 2009;30(8):1551–9.

[54] Cheema U, Chuo CB, Sarathchandra P, Nazhat SN, Brown RA. Engineering functional collagen scaffolds: cyclical loading increases material strength and fibril aggregation. Adv Funct Mater 2007;17(14):2426–31.

Biomaterials 32 (2011) 1080–1090

Contents lists available at ScienceDirect

Biomaterials

journal homepage: www.elsevier.com/locate/biomaterials

Irreversible optical clearing of sclera by dehydration and cross-linking

Yuji Tanaka [a,b], Akira Kubota [a], Masayuki Yamato [b], Teruo Okano [b], Kohji Nishida [a,c,*]

[a] Department of Ophthalmology and Visual Science, Tohoku University Graduate School of Medicine, 1-1 Seiryo-machi, Aoba-ku, Sendai, Miyagi 980-8574, Japan
[b] Institute of Advanced Biomedical Engineering and Science, Tokyo Women's Medical University, TWIns, 8-1 Kawada-cho, Shinjuku-ku, Tokyo 162-8666, Japan
[c] Department of Ophthalmology, Osaka University Medical School, Yamadaoka 2–2, Suita 565-0871, Japan

ARTICLE INFO

Article history:
Received 13 July 2010
Accepted 1 October 2010
Available online 4 November 2010

Keywords:
Collagen structure
Cross-linking
Soft tissue biomechanics
Transparency
Cornea
Sclera

ABSTRACT

This study manipulates both clear cornea and opaque sclera by two dehydration processes for revealing the relationship between altered tissue structures and change in optical functions. In contrast to the high levels of light scattering in dehydrated tissues by critical point dry, a simple dehydration at 4–8 °C effectively and significantly improved their visible-light transmission, even in the sclera, with accompanying dense fiber packing. Further improvement in visible-light transmission, from 40–50% to 80–90%, has been achieved by flatting tissue surface with cover glasses during dehydration at low temperature. Such optical clearing of sclera by dehydration is reversible. However, chemical cross-linking effectively stabilizes their densely packed microscopic structures and visible-light transmission at over 50% irreversibly, even at wet conditions. Interestingly, the repetition of both low temperature dehydration/cross-linking treatments effectively reduced the required amounts of cross-linking reagents to keep a high transparency. Wet transparent cross-linked sclera can also show a characteristic strong tensile strength. Furthermore, rabbit corneal epithelium has regenerated on the transparent sclera with cross-linking *in vitro*.

1. Introduction

Structural characters in tissues are strongly linked with their naturally intrinsic functions. Recently, several studies have reported that tissue intrinsic light scattering properties can be altered artificially. Reversible optical clearing of non-light transmissive fibrous tissues such as skin have been investigated with chemical reagents (i.e. dimethyl sulfoxide and glycerol) [1–4], and mechanical compression [5,6] *in vitro* and *in vivo* as an attempt for future optical therapies and diagnosis (i.e. optical coherence tomography). Several researchers suggest that the potential mechanisms of optical clearing are thought to be dehydration and refractive index matching in matrix. These methods also cause structural changes in tissues, especially the significant reduction of thickness by compression, indicating the potential importance of structure for optical clearing.

On the other hand, one of the highly illustrative *in vivo* examples of structural difference affecting optical character is the relationship between transparent cornea and cloudy sclera, the same collagen fibrous membranes with approx. 500 μm thick, adjoined on the surface of the eye. In the cornea, collagen molecules self-assemble into fibrils with a remarkably uniform diameter (31 nm, in humans), organizing the tissue-specific lateral arrangement of collagen fibrils with some degree of short-range spatial order [7–10]. In contrast, scleral coat is composed of disturbed fiber structures with inhomogeneous microfibril diameter ranging from 30 nm to 300 nm [8]. Such the difference in spontaneous structures has a huge bearing on their completely opposite characters against visible-light transmission *in vivo*.

The principal purpose of this study is to clarify specific structures that permit the visible-light transmission in the tissues. This study applied two types of dehydration processes, critical point drying and low temperature drying at 4–8 °C, to give a change in structures in both cornea and sclera *ex vivo*. The former method is widely applied to dehydrate biological tissues with maintaining their original structures before their scanning electron microscope observations [11–13]. In contrast, the latter method was reported as a simple method to vitrify boiled white egg [14] and purified atelocollagen solution [15,16]. Interestingly vitrified white egg and atelocollagen are known to permit visible-light transmission, but these methods have never been applied for the optical clearing of tissues. In the field of ophthalmology, tissues visible-light transmission is important, but there was assumption that the cornea was clear and sclera was clouded *in vivo*. Even clear cornea *in vivo* is gradually swelled and clouded in aqueous solution after its isolation. This study verified the cornea and sclera treated by the two processes described above from molecular level to macroscopic level by UV/Vis-spectroscopy and electronic microscopy.

* Corresponding author. Department of Ophthalmology, Osaka University Medical School, Yamadaoka 2–2, Suita 565-0871, Japan. Tel.: +81 6 6879 3450/3451; fax: +81 6 6879 3459.
E-mail address: knishida@ophthal.med.osaka-u.ac.jp (K. Nishida).

0142-9612/$ – see front matter © 2010 Elsevier Ltd. All rights reserved.
doi:10.1016/j.biomaterials.2010.10.002

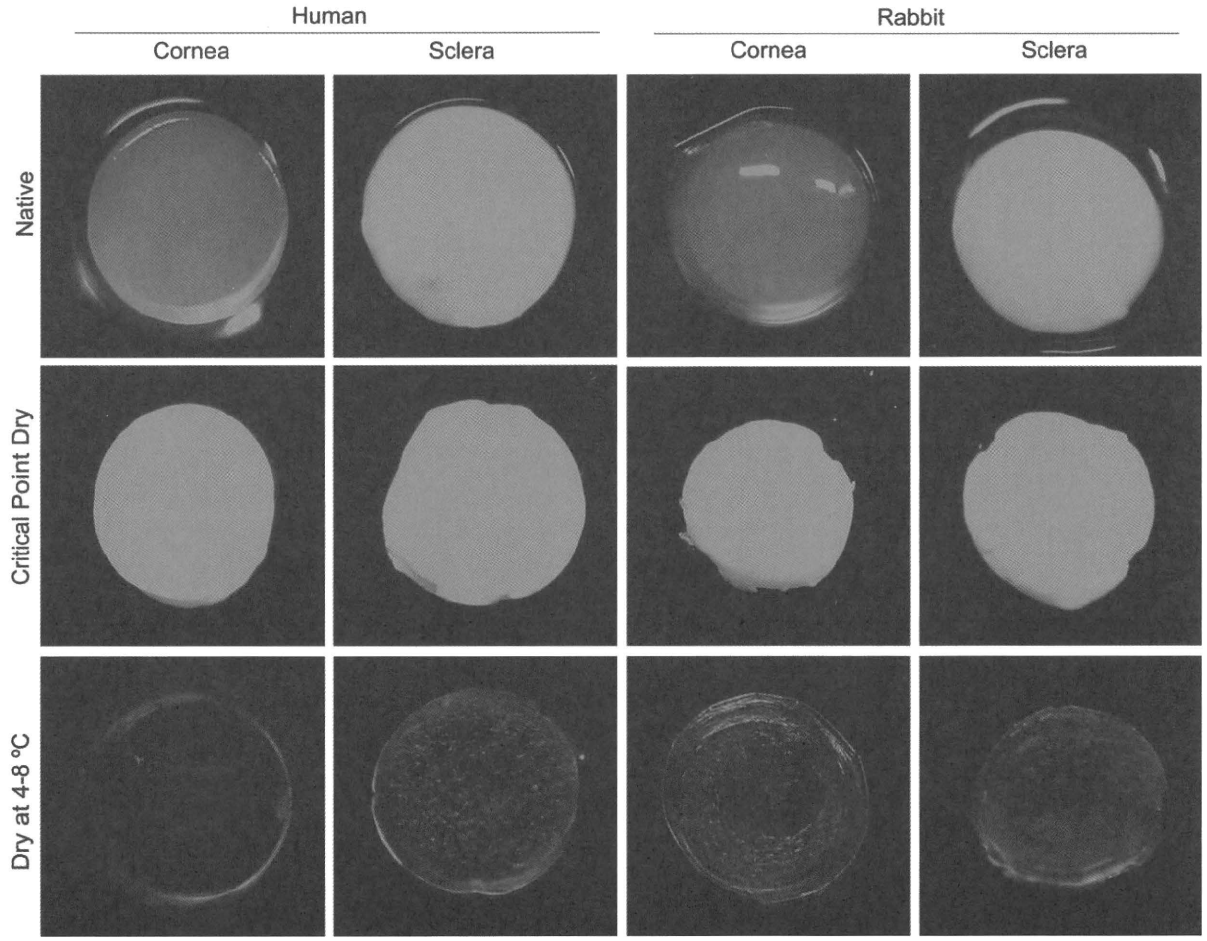

Fig. 1. Photography of cornea and sclera treated by drying processes. Human corneas, human scleras, rabbit corneas, and rabbit scleras are shown on the first, second, third, and forth column, respectively. Native wet tissues, critical point dried tissues, and low temperature dried tissues are shown on the first, second, and third row, respectively.

Furthermore, this study also examined the following experiments to maintain the high visible-light transmission of dehydrated tissues, because the dried tissues swelled and clouded by rehydration in aqueous solution. As an additional investigation for structural contribution to optical clearing and further developments for the expansion of its possible applications, chemical cross-linking was performed on transparent dried sclera for fixing its specific structural character. It is extremely important to maintain the transparency irreversibly in aqueous solution, because the cornea of the living body always contact with aqueous humor in the anterior chamber. Moreover, transparent sclerotic coat could be used as a substitution for the cornea, and the tissue will be an ultimate solution for the donor shortage of corneal stroma. This study investigated corneal epithelial regeneration on irreversibly optically cleared sclera for examining their cell compatibility for further ocular application.

2. Materials and methods

2.1. Dry treatments of cornea and sclera

Human cornea and sclera were prepared from donated corneoscleral buttons (Eye Bank, SightLife, Seattle, USA). Rabbit cornea and sclera were obtained from Japanese white rabbit eyeball (Kitayama Labes, Ina, Japan). Tissues were trepanned (3 mm in diameter) and cut into adequate peaces for following analysis. All tissues were soaked in normal saline and followed by immersion in distilled water. Critical point dry or natural dry was applied for these rinsed tissues. Critical point dry was performed with a critical point dryer (HCP-2) (Hitachi, Hitachi, Japan) with carbon dioxide. In this case, the tissue was treated with elevated ethanol and isoamyl

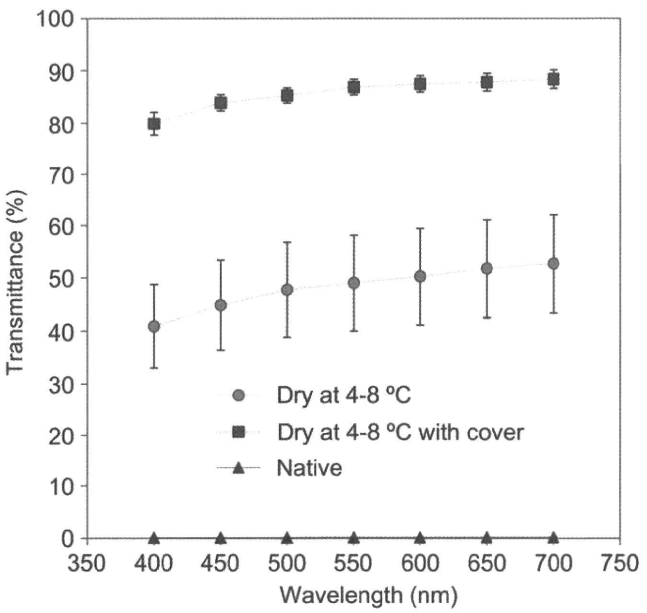

Fig. 2. Transmittance of rabbit sclera prepared by drying process. The closed triangles, squares, and circles represent wet sclera, sclera dried at 4–8 °C, and a sclera dried at 4–8 °C with cover, respectively.

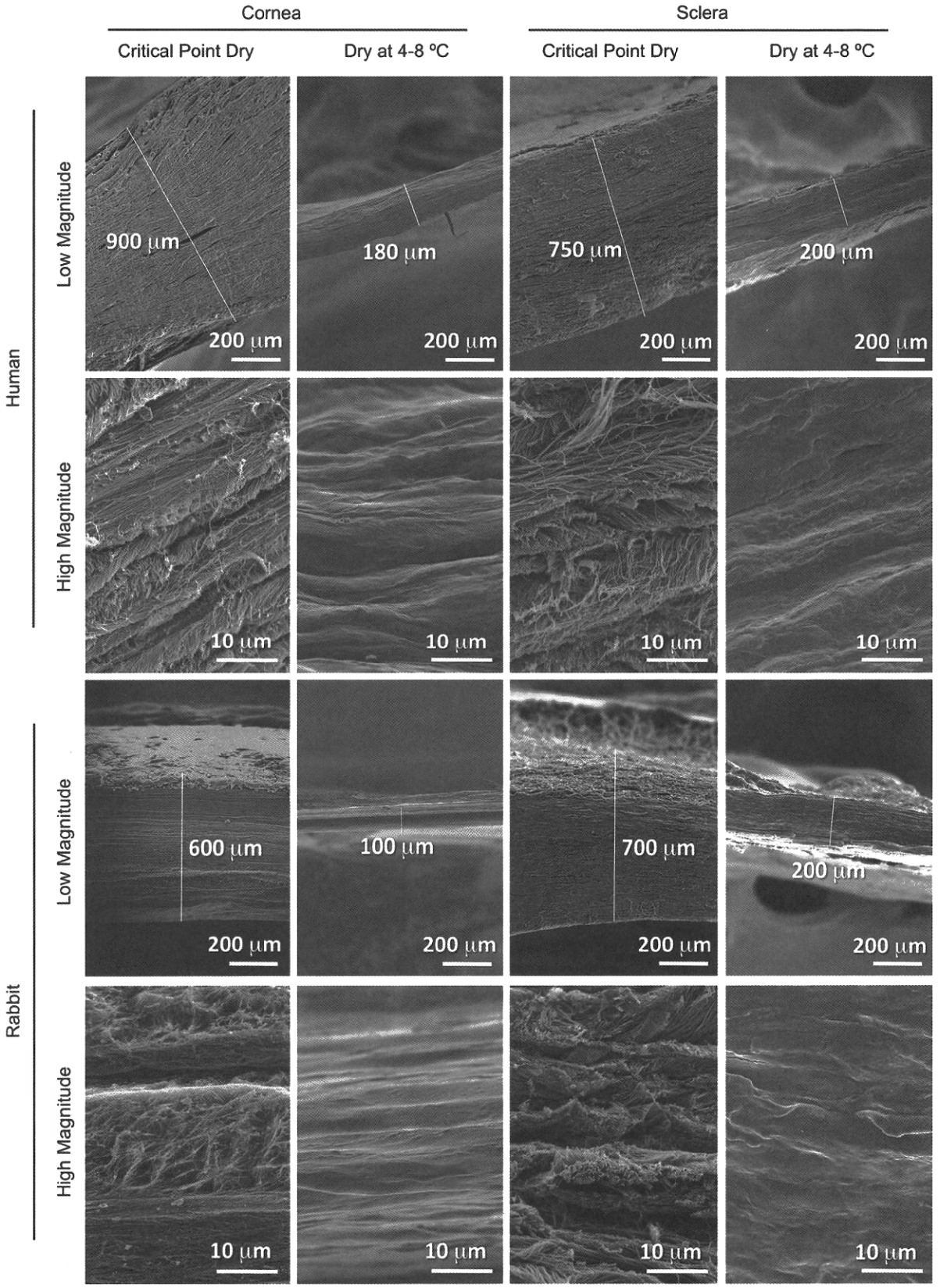

Fig. 3. SEM imaging of fiber structure on the cross-section of corneal stroma and sclera which were dried by low temperature dry treatment or critical point dry treatment.

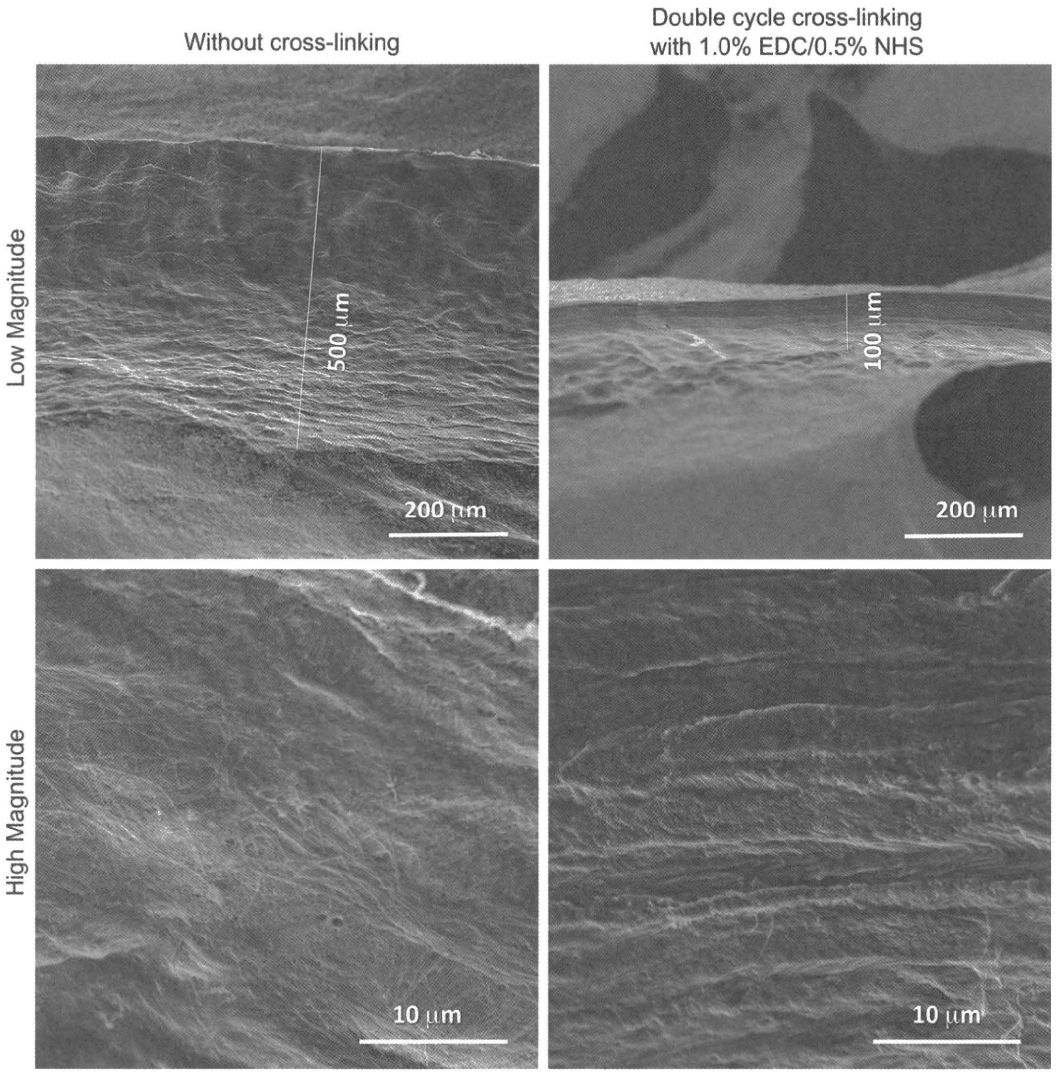

Fig. 6. SEM imaging of fiber structure on the cross-section of human and rabbit sclera which treated with double-cycle optical clearing (low temperature dry and cross-linking) with or without cross-linking.

processes (Fig. 1). Trepanned cornea swelled and lost its transparency in PBS within several minutes, but still clearer than that of wet sclera (the first row, Fig. 1). Visible-light transmission of the swelled cornea was decreased by critical point dry treatment to the level of sclera (the second row, Fig. 1). In contrast, the transparency of all tissues including sclera turned to be transparent by low temperature drying treatment at cold room (4–8 °C) for one day (the third row, Fig. 1).

The quantitative analysis of visible-light transmission of rabbit sclera shows a significantly increase in visible-light transmission to 40–50% from 0 to 1% by low temperature drying treatment in cold room (4–8 °C) (Fig. 2). For the further improvement of visible-light transmission, applied glass covers were used during low temperature drying treatments for flatting the irregular surface. The rabbit sclera gradually turned to be transparent from the peripheral part to central part for 1–2 weeks. Interestingly, the visible-light transmission of the resultants with cover glass was significantly improved up to 80–90%.

SEM analysis of the cross-section of dried tissue clearly visualized differences in the tissue structures of both thickness and microscopic fiber morphology in both critical point dried tissues and tissues dried at low temperature without glass cover (Fig. 3). All critical point dried tissues exhibited more than 600 μm thickness with lacunal structure. In contrast, all optical transmission tissues dried at low temperature exhibited more than 200 μm thickness with dense fiber packing.

Both hydration processes with low temperature and chemical cross-linking treatments affected the transparency of human sclera as shown in Fig. 4A The samples without dry treatment were clouded regardless of cross-linking agents (the second row, Fig. 4A). However, all samples hydrated with chemical cross-linking after low-temperature drying exhibited a color change and an improvement in light transmission (the first row, Fig. 4A), although the light transmission decreased to the level of native sclera without any cross-linking reagents (the control, the first row on the 5th column, Fig. 4A). Color of GA treated sclera was yellow, but no color change was found in the sample without dry process. Additionally, the effect of concentration of EDC/NHS on dehydrated sclera at low temperature was examined (Fig. 4B). The concentration of cross-linking reagents lower than 20%/10% (EDC/NHS) allowed the transparency of wet cross-linked sclera to increase with increasing cross-linking reagents, but the concentration over 40%/20% (EDC/NHS) allowed the sclera to be significantly clouded.

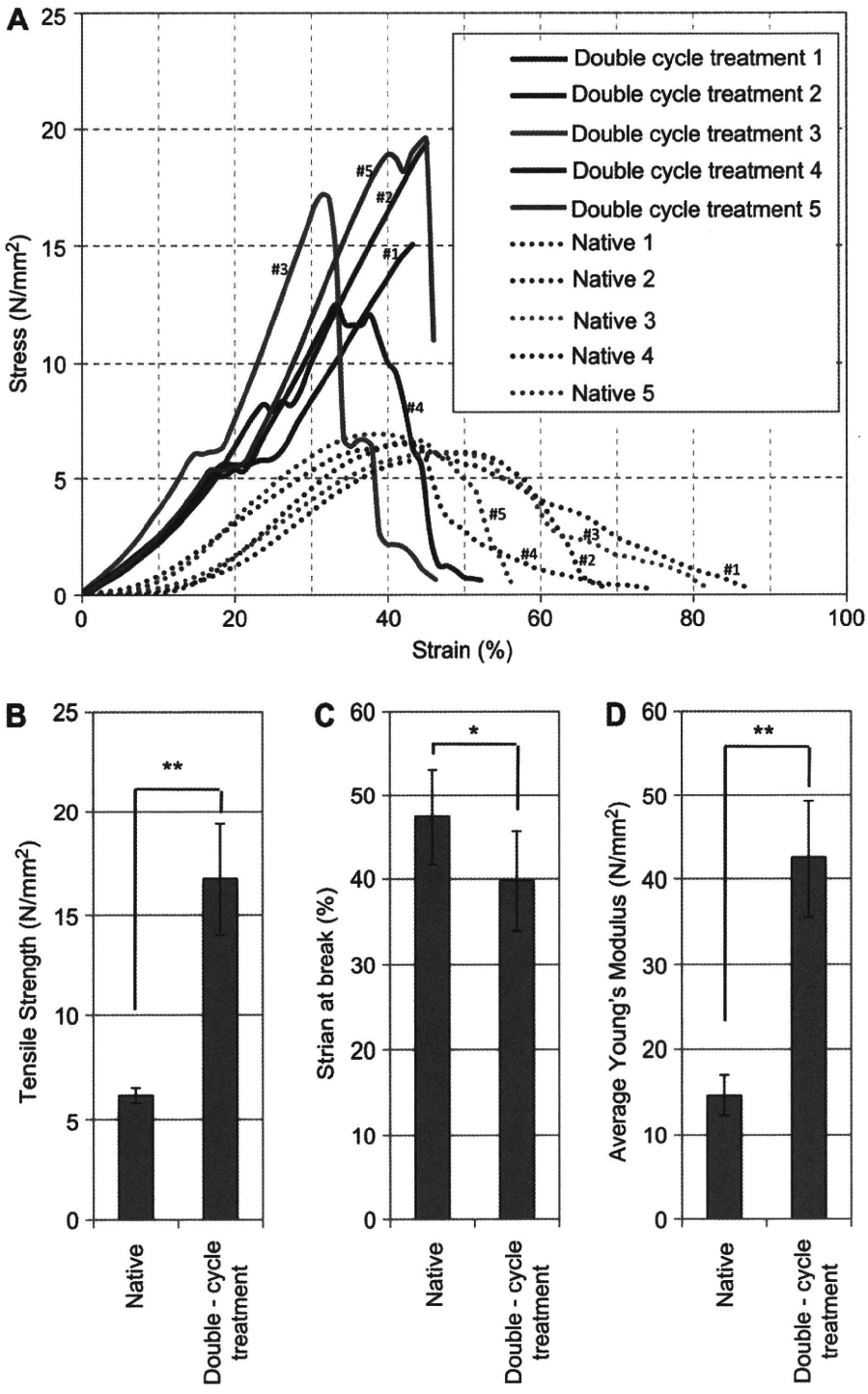

Fig. 7. Effect of double-cycle optical clearing (low temperature dry and cross-linking) on the mechanical properties of sclera. Stress–strain curves (A), tensile strength (B), strain at break (C), and average Young's modulus before break (D). $n = 5$, one-tail unpaired t-test (* = significant difference $p < 0.05$, ** = significant difference $p < 0.01$).

As a further quantitative study on these optical clearing treatments (low-temperature dry, chemical cross-linking, and washing) for improving transparency at wet conditions, these optical clearing processes were repeated on rabbit sclera (Fig. 5A). The control sclera swelled and clouded in PBS (the first column, Fig. 5B). The transparency of the sclera in PBS increased with swelling with increasing the concentration of cross-linking reagent (Fig. 5B and C). By the single-cycle treatment of low temperature drying/chemical cross-linking, the transparency of the rabbit sclera increased up to 50% with increasing the concentration of cross-linking reagent. Repetition of the cycle treatment effectively increased the transparency when the concentration of EDC/NHS was 0.01%/0.005%, 0.1%/0.05%, and 1.0%/0.5%. In contrast, the transparency decreased when the concentration of EDC/NHS was 10.0%/5.0%. No significant differences in transparency were found between the double and the triple-cycle treated scleras. The maximum transparency of sclera was higher than 55%, when sclera was treated with the double or triple-cycle process with 1% EDC/0.5% NHS. The double-cycle